Numerical study of cellular detonation wave reflection over a cylindrical concave wedge

Xueqiang Yuan [a,b], Jin Zhou [a]*, Xiaocheng Mi [c], Hoi Dick Ng [b]

[a]*Science and Technology on Scramjet Laboratory, National University of Defense Technology, Changsha 410073, China*

[b]*Department of Mechanical, Industrial and Aerospace Engineering, Concordia University, Montréal, Québec H3G 1M8, Canada*

[c]*Department of Mechanical Engineering, McGill University, Montréal, Québec H3A 2K6, Canada*

Abstract

Numerical simulations were performed to study reflection of a stable detonation wave with regular cellular patterns over a cylindrical concave wedge. The dynamics of this reflection phenomenon was described by the two-dimensional reactive Euler equations with a two-step induction-reaction kinetic model and solved numerically using the adaptive mesh refinement code AMROC. The effects of various parameters on the reflection evolution were analyzed in detail. The results indicate that the reflection-type transition of a stable cellular detonation is similar to that of a planar shock wave over a concave wedge. The triple-point trajectory resulted from the Mach reflection when the cellular detonation first encounters the concave wedge coincides with that of the planar shock propagating for the case with the same incident Mach number. As the effective wedge angle continuously increases, the Mach reflection of cellular detonation deviates from that of a planar shock with a reduced Mach stem height, and the transition from Mach to regular reflection occurs at a smaller angle. This observation is further explored by adopting the length-scale (or "corner-signal") concept, examining the velocity variation of corner signals generated by fluid particles around the wedge tip. The reflection dynamics is described qualitatively by the ratio of two length scales characterizing the detonation structure, namely, the induction-zone and reaction-zone lengths. The increase of these length scales raise the Mach stem height and transition angle. Apart from the detonation length scales, the wedge curvature radius is found to have an opposite effect since the increase of radius expands the region where the corner signals are generated by the particles behind the induction zone, and makes the corner signals persist in a state with attenuating velocity.

Keywords: Cellular detonation; Regular/Mach reflection; Cylindrical wedge; Length-scale

effects

1. Introduction

A rotating detonation engine (RDE) is a detonation-based propulsion device which can realize continuous detonative combustion and provide high-frequency stable thrust once initiated. It has become the principal focus in the recent development of hypersonic propulsion systems [1-2]. A number of fundamental research closely related to RDE can also be found in the literature analyzing the dynamics of gaseous detonations bounded by an inert compressible layer, e.g., [3-4]. In the annular combustion chamber of a rotating detonation engine (RDE), as conceptually illustrated in Fig. 1(a), a circumferentially propagating detonation wave experiences lateral expansion in the axial direction of the engine under the confinement of two cylindrical chamber walls. To better examine the effect of wave-wall interaction on the propagation behavior in three-dimensional RDE geometries, some recent studies [5-12] have focused on detonation propagation in a two-dimensional curved channel, see Fig. 1(b). A detonation wave propagating in such a curved channel, as shown in Fig. 1(c), is subject to a diffraction along the convex inner wall and a compression along the concave outer wall. Kudo et al. [5] and later researchers [6-8, 10, 12] have repeatedly demonstrated that the criterion for a steady propagation is governed by the inner wall curvature (or, equivalently, arc radius) determining whether the diffraction is sufficiently intense to locally quench the detonation wave. In the cases where detonation failure occurs near the inner wall, the detonation might be re-initiated as a result of wave reflection from the concave outer wall [9]. Thus, an in-depth investigation on the dynamics of a cellular detonation wave being reflected from a concave surface is motivated.

In the current study, the reflection of a weakly unstable incident detonation wave with regular cellular patterns over a 90° cylindrical concave wedge (as shown in Fig. 2) is placed under scrutiny via computational simulations. It is worth mentioning that a number of investigations can be found in the literature on the detonation wave reflection over wedges, but mostly in the planar geometry. For this configuration, the early studies treated the detonation front as a strong reactive discontinuity neglecting the reaction zone thickness [13-15] and employed the reactive three-shock theory [16-17] or Chester–Chisnell–Whitham (CCW) [18-20] theory to examine the detonation reflection characteristics. Nevertheless, experimental observations have shown that the Mach reflection triple-point trajectory of a detonation wave is curved, indicating that the Mach reflection is not self-similar [21-22] and thus, the aforementioned theories for pseudo-steady flow cannot fully describe the reflection of detonation waves. Shepherd et al. [23] explained the self-dissimilarity of detonation wave reflection by introducing the concept of frozen and equilibrium limits. They assumed that the Mach reflection process of a detonation wave was controlled by the non-reactive or "frozen" dynamics in the near field, but in the far field, the process was controlled by the reacted or "equilibrium" dynamics. The effect of frozen and equilibrium limits was confirmed by Fortin et al. [24] and Li et al. [25-27] with experiments and numerical simulations, respectively. Li et al. [27] also pointed out that if the reaction zone length is sufficiently small compared with the propagation distance, the Mach reflection would approach to self-similarity in the far field, and the distance from the wedge tip to where the triple-point trajectory becomes straight, i.e., the Mach reflection approaches self-similarity, was quantified to be 6-10 times the characteristic detonation cell width.

For the unsteady shock reflection over cylindrical concave wedges, both the modified Chester-Chisnell-Whitham (CCW) theory and the length-scale (or "corner-signal") concept [28] were employed to construct models to predict the Mach stem height H_{m} as well as the transition wedge angle of Mach-to-regular reflection (MR-RR) [29-32], and the reflection of a weak shock wave was investigated [33]. In essence, the length-scale concept considers a corner signal generated from the initial point on the cylindrical surface communicating with the incident shock wave in determining the MR-RR transition process. Apart from single cylindrical wedges, the reflection process over combined wedges, e.g., combination of convex-concave cylindrical reflectors, has also drawn more attention in recent years [34-37].

In this study, the objective is to analyze in detail the reflected detonation wave structure and the transition between various types of reflection. Aforementioned studies on unsteady shock reflection over a concave wedge provide benchmark scenarios for the current problem of detonation reflection [26]. The simulation results of detonation reflection were thus compared with those of an inert shock. The length-scale concept developed by Hornung et al. [28] was invoked to interpret the evolution of the reflected detonation structure. The effects of various chemical kinetic parameters and wedge curvature radii on the dynamics of detonation reflection were further examined and discussed.

2. Computational model and numerical scheme

2.1 Computational model

It is worth noting that the effects of viscosity and diffusion are found to influence self-similar shock wave solutions [38] and the propagation dynamics of highly unstable detonation [39-41]. For instance, recent research [38] has indicated that for the Mach reflection of a detonation wave, the viscosity near the wall can affect the flow by generating a small vortex behind the Mach stem. However, the effect on the global structure of Mach reflection triple-point and the triple-point trajectory is minimal compared with the inviscid case. In this study, the focus is on the length-scale effects and a weakly unstable detonation is considered. Hence, viscous and diffusion effects are neglected in the detonation flow. Thus, the two-dimensional reactive Euler equations were used as the governing equations, and in order to investigate the effect of the detonation reaction structure, a two-step chemical kinetic model was applied for the chemical reaction, which allows one to vary independently the characteristic reaction length scales. All flow variables were non-dimensionalized with respect to the unburned mixture states ahead of the detonation front as follows:

$$\rho=\frac{\tilde{\rho}}{\tilde{\rho}_0},\quad p=\frac{\tilde{p}}{\tilde{p}_0}, T=\frac{\tilde{T}}{\gamma\tilde{T}_0}, u=\frac{\tilde{u}}{\sqrt{\mathrm{R}\tilde{T}_0}}, v=\frac{\tilde{v}}{\sqrt{\mathrm{R}\tilde{T}_0}}, q=\frac{Q}{\mathrm{R}\tilde{T}_0} \tag{1}$$

where the symbol (~) represents dimensional quantities and the subscript (0) denotes the quantities ahead of the detonation front. The variables ρ, p, u, v, T, and Q represent the density, pressure, velocity in *x*-direction and in *y*-direction, and the heat release parameter, respectively.

The non-dimensional governing equations have the form:

$$\frac{\partial\rho}{\partial t}+\frac{\partial(\rho u)}{\partial x}+\frac{\partial(\rho v)}{\partial y}=0 \tag{2}$$

$$\frac{\partial(\rho u)}{\partial t}+\frac{\partial(\rho u^2+p)}{\partial x}+\frac{\partial(\rho uv)}{\partial y}=0 \tag{3}$$

$$\frac{\partial(\rho v)}{\partial t}+\frac{\partial(\rho uv)}{\partial x}+\frac{\partial(\rho v^2+p)}{\partial y}=0 \tag{4}$$

$$\frac{\partial E}{\partial t}+\frac{\partial((E+p)u)}{\partial x}+\frac{\partial((E+p)v)}{\partial y}=0 \tag{5}$$

$$\frac{\partial(\rho y_{\mathrm{I}})}{\partial t}+\frac{\partial(\rho u y_{\mathrm{I}})}{\partial x}+\frac{\partial(\rho v y_{\mathrm{I}})}{\partial y}=\omega_{\mathrm{I}} \tag{6}$$

$$\frac{\partial(\rho y_{\mathrm{R}})}{\partial t}+\frac{\partial(\rho u y_{\mathrm{R}})}{\partial x}+\frac{\partial(\rho v y_{\mathrm{R}})}{\partial y}=\omega_{\mathrm{R}} \tag{7}$$

the parameters y_{I} and y_{R} indicate the induction and reaction progress variables of the reaction model.

The total energy E is given by

$$E = \frac{p}{\gamma - 1} + \frac{\rho\left(u^2 + v^2\right)}{2} - \rho y_{\mathrm{R}} q \tag{8}$$

The flow system consists of a calorically perfect gas with a constant ratio of specific heat and an equation of state:

$$p = \rho T \tag{9}$$

For this ideal flow model, the CJ detonation Mach number can be obtained by

$$M_{\mathrm{CJ}} = \frac{D}{c_0} = \left[\left(1 + \frac{\gamma^2 - 1}{\gamma} q\right) + \sqrt{\left[\left(1 + \frac{\gamma^2 - 1}{\gamma} q\right)^2 - 1\right]}\right]^{\frac{1}{2}} \tag{10}$$

Details of the two-step induction-reaction kinetic model used in this work are described in [42]. The first step is a thermally neutral induction step with no energy release. The Arrhenius rate ω_{I} is given by

$$\omega_{\mathrm{I}} = H\left(1 - y_{\mathrm{I}}\right) \rho k_{\mathrm{I}} \exp\left[E_{\mathrm{I}}\left(\frac{1}{T_{\mathrm{S}}} - \frac{1}{T}\right)\right] \tag{11}$$

where T_{S} is the post-shock temperature behind the leading front, and $H\left(1 - y_{\mathrm{I}}\right)$ is a step function defined as

$$H\left(1 - y_{\mathrm{I}}\right) = \begin{cases} 1 & \text{if} \quad y_{\mathrm{I}} < 1 \\ 0 & \text{if} \quad y_{\mathrm{I}} = 1 \end{cases} \tag{12}$$

As the induction step terminates, the reaction step with energy release starts. The rate of this step ω_{R} is given by

$$\omega_{\mathrm{R}} = \left(1 - H\left(1 - y_{\mathrm{I}}\right)\right) \rho k_{\mathrm{R}} \left(1 - y_{\mathrm{R}}\right) \exp\left(\frac{-E_{\mathrm{R}}}{T}\right) \tag{13}$$

The variables E_{I}, E_{R} correspond to the activation energies of each step. Consistent with the previous study [25, 42], we define the dimensionless activation energies as $\varepsilon_{\mathrm{I}} = \frac{E_{\mathrm{I}}}{T_{\mathrm{S}}}$ and $\varepsilon_{\mathrm{R}} = \frac{E_{\mathrm{R}}}{T_{\mathrm{S}}}$, and generally $\varepsilon_{\mathrm{I}} > \varepsilon_{\mathrm{R}}$. The terms k_{I} and k_{R} represent the induction and reaction pre-exponential rate constants, which control the thickness of the induction and reaction zones, i.e., Δ_{I} and Δ_{R}, respectively. In this paper, the length of the induction zone Δ_{I} is chosen as the unity reference length scale, i.e., Δ_{I}=1, so it has the relation that $k_{\mathrm{I}} = -u_{\mathrm{vn}}$, where u_{vn} is the particle velocity behind the shock front in the shock-fixed frame for the CJ detonation. As there is no specific definition of the reaction zone, the reaction length Δ_{R} is defined as the distance between the end of the induction zone and the location where the reaction progress y_{R} reaches 99.9%. Hence, the thickness of a detonation wave Δ is given by $\Delta = \Delta_{\mathrm{I}} + \Delta_{\mathrm{R}}$, and the ratio of the length Δ_{I} and Δ_{R} is defined as $\phi = \frac{\Delta_{\mathrm{R}}}{\Delta_{\mathrm{I}}}$. The state parameters of a ZND detonation wave based on the two-step chemical kinetic model are shown schematically in Fig. 3. Using the aforementioned chemical kinetic parameters, the stability parameter χ defined as $\chi = \varepsilon_{\mathrm{I}} \frac{\Delta_{\mathrm{I}}}{\Delta_{\mathrm{R}}}$ by Ng et al. [42] can be evaluated. Detonation waves with a small value of χ are generally stable. In the present study, the condition $\Delta_{\mathrm{R}} >> \Delta_{\mathrm{I}}$ were ensured to form a stable cellular detonation wave with a low degree of cellular instability.

2.2 Numerical method and computational setup

In order to capture the detailed detonation structure, the simulations require a high-resolution mesh distributed around the wave front, while other areas with relatively mild flow behavior can be resolved with a coarser grid to reduce computational cost. In this work, the structured adaptive mesh refinement (SAMR) code AMROC developed by Deiterding [43] was employed for the high-resolution simulations. As to the numerical methodology, the second-order accurate MUSCL-TVD method with the Van Albada limiter was adopted for the spatial discretization, and the second-order accurate Runge-Kutta technique [44] was applied for the temporal discretization with the Courant-Friedrichs-Lewy (CFL) number of 0.95. The first-order accurate Godunov splitting method was used to integrate the reaction source term.

The simulations of detonation reflection over a cylindrical concave wedge were conducted in a two-dimensional computational domain, as shown in Fig. 4. Reflecting boundary with slip conditions were used on both the upper and bottom wall as well as the concave wedge. Since the Cartesian grids created by the SAMR method cannot line the curved boundary completely, the walls of the curved section were encircled by several layers of ghost cells [45], and the corresponding boundary conditions were constructed by interpolating these cells. The cells around where the detonation wave front stands were refined with the highest refinement level, as presented in Fig. 5 (ghost cells are invisible). Transmissive conditions were adopted on the left and right boundaries.

In the present study, a constant isentropic exponent of $\gamma = 1.44$ was used. The variables investigated in this work include the activation energy ε_{I} and ε_{R}, the CJ detonation Mach number M_{CJ}, the length ratio ϕ, and the curvature radius of the concave wedge R_0. To initialize the computation, a one-dimensional ZND detonation wave under the specified initial conditions was placed initially at a distance three times the detonation thickness Δ from the left boundary in order to insure the state parameters on the inlet to be the values behind the sonic plane. A buffer section in the computational domain allows the detonation wave to propagate approximately a hundred detonation thicknesses Δ for the cellular instability to be fully developed before entering the curved wedge and ensures that the left boundary does not influence the detonation wave front dynamics. Figure 6 shows the numerical soot foil developed by the incident cellular detonation wave under the conditions of $\varepsilon_{\mathrm{I}} = 4$, $\varepsilon_{\mathrm{R}} = 1$, $M_{\mathrm{CJ}} = 5.4$, and $\phi = 25$, giving a stability parameter of $\chi = 0.16$. The approximate sizes of one detonation cell are also provided in the figure. Referring to [42], this corresponding low stability parameter should give rise to a detonation wave with regular cellular structure, which is consistent with the regular cellular patterns observed on the numerical soot foil.

2.3 Grid resolution study

Since the overall computational cost cannot be underestimated even when the SAMR method is applied, an optimal combination of mesh adaption flag parameters should be established. Here, we used the threshold values on density, temperature, and pressure of $\tau_{\rho} = 0.05$, $\tau_{T} = 5\times10^{2}$, and $\tau_{p} = 5\times10^{4}$, respectively, where τ represents the scaled gradient of each parameter. A flagging efficiency [43] of 0.9, representing the percentage of flagged cells against the entire level cells, was used for SAMR grid generation.

To investigate the effect of grid resolution on the simulations, a series of verification computations for detonation reflection over a concave wedge with different mesh refinement strategies were conducted with the conditions of $\varepsilon_{\mathrm{I}} = 4$, $\varepsilon_{\mathrm{R}} = 1$, $= 5.4$, $\phi = 25$, and $R_{0} = 750$. In this paper, the trajectory of Mach reflection triple-point and the angle of Mach reflection-regular reflection (MR-RR) transition are most significant for analyzing the reflection characteristics, so the accuracy of these parameters should be insured primarily. Figure 7 presents the numerical soot foils, the corresponding trajectories of the triple-point as well as the pressure curves along the fixed height of $y = 140$ at the same time instant (crossing the Mach stem) for three different resolutions, and Table 1 lists the MR-RR transition angle as well as the CPU time for each resolution with 36 CPU cores. It can be observed that both the triple-point trajectory and the pressure curve are not very sensitive to these three chosen grid resolutions, and the transition angles of all cases are essentially equivalent. Considering the computational cost, the second-highest resolution of $\Delta x_{\min} = 32$ pts/Δ_{I} was applied for all the following simulations.

3. Results and analysis

3.1 Detonation reflection process over a cylindrical concave wedge

The detonation wave reflection process and parameters defined for the present study are described schematically in Fig. 8. It should be noted that, to define different parameters, the Mach stem is assumed to be straight and perpendicular to the wedge in the present work. Therefore, H_{m} and θ_{w} are equal to the length of the Mach stem and the tangential wedge angle corresponding to where the Mach stem stands, respectively. The parameters H_{m}, θ_{w}, and θ_{w}^{*}, which reveal basic characteristics of the reflection process, are the key features for measurement and analysis.

Similar to shock reflection [17], the transition between various reflection types, from direct-Mach reflection (DiMR) to stationary-Mach reflection (StMR) to inverse-Mach reflection (InMR) and finally to transitioned regular reflection (TRR), occurs throughout the whole detonation reflection process. The numerical soot foil in Fig. 9 presents the transition between different reflection types as well as the variation of the Mach stem, corresponding to the conditions of ε_{I} = 4, ε_{R} = 1, M_{CJ} = 5.4, ϕ = 25, and R_0 = 750. Initially the detonation cells have almost the same size, forming a stable cellular detonation wave. Upon reflection, as the cellular patterns are being affected by the compression, the cells created by the Mach stem near the wedge have a smaller size while the cell size in the upper area remains unchanged. Thus, an evident boundary line on the soot foil separating these two areas represents the trajectory of the Mach reflection triple-point. In this paper, the Mach stem height H_{m} was obtained by extracting the coordinates of points on this trajectory at fixed distance intervals, and the transition angle θ_{w}^{*} can also be confirmed since the MR-RR transition makes the pressure at the transition point reach a maximum, as the partially enlarged detail in Fig. 9 shows.

The specific detonation wave structure of all different reflection types in one simulation case is displayed in Fig. 10. When the detonation wave just propagates through the wedge tip, the Mach stem position corresponds to a small tangential wedge angle θ_{w}, leading to the reflection type DiMR. As shown in Fig. 10(a), the angle between the flow vector under the Mach reflection triple-point and the wedge surface where the Mach stem stands has a positive value, which indicates that the fluid behind the Mach stem has a direction deviating from the wedge. Therefore, the Mach stem is growing while the detonation wave propagates, i.e., $\frac{\mathrm{d}H_{\mathrm{m}}}{\mathrm{d}\theta_{\mathrm{w}}} > 0$. As the propagation continues, the increase of θ_{w} makes the direction of the flow vectors begin to deviate towards the wedge correspondingly, and the Mach stem cannot grow further when the flow vectors are parallel to the wall, i.e., $\frac{\mathrm{d}H_{\mathrm{m}}}{\mathrm{d}\theta_{\mathrm{w}}} = 0$, forming a structure of StMR, as presented in Fig. 10(b). Due to the constant change of θ_{w} along with the wave propagation, the StMR structure is transient and has a maximum Mach stem length. As θ_{w} increases further, the angle between the flow vectors and the wall becomes negative, which shortens the Mach stem with $\frac{\mathrm{d}H_{\mathrm{m}}}{\mathrm{d}\theta_{\mathrm{w}}} < 0$. The InMR is then realized as illustrated in Fig. 10(c). Finally, the Mach stem disappears as the Mach reflection transits to regular reflection, as shown in Fig. 10(d).

3.2 Comparison between detonation and planar shock wave reflection

As introduced in Sect. 1, using the length-scale (or "corner-signal") concept [28], Ben-Dor and Takayama et al. [17, 30-32] predicted the transition angle θ_{w}^{*} of shock wave reflection over cylindrical concave wedges. The length-scale (or "corner-signal") concept suggests that to form a Mach reflection structure with finite length, a corner signal, which is a physical length scale signal generated by the fluid particles around the wedge tip, must be communicated to the reflection triple-point, otherwise regular reflection will result.

Figure 11 illustrates schematically a shock wave Mach reflection prior to its MR-RR transition occurring at the point *Q*. Since the transition occurs where the Mach reflection cannot exist, the Mach reflection in the vicinity of point *Q* (just before transition) represents the extreme position where the corner-generated signals can communicate with the triple-point. The signals propagate with a velocity of $u_{\mathrm{s}} = u + a$, where u is the flow velocity and a is the local speed of sound. Considering that the reflected shock wave becomes very weak when it approaches the wedge surface, it implies that the flow properties do not change significantly while passing through the reflected wave. Therefore, the velocity u_{s} can be approximated by a fixed value as:

$$u_{\mathrm{s}} = u_1 + a_1 \tag{14}$$

where u_1 and a_1 are the flow velocity and the local sound speed behind the incident shock wave, respectively. If Δt is the time required for the incident shock wave to travel from the wedge tip *A* to the transition point *Q*, then the distance S that the corner-generated signals have propagated can be obtained by:

$$S = \left(u_1 + a_1\right)\Delta t \tag{15}$$

In Ben-Dor's model, the propagation path of the corner-generated signals is assumed to be along the wedge surface, which indicates that

$$S = R_0 \theta_{\mathrm{w}}^{*} = \left(u_1 + a_1\right)\Delta t \tag{16}$$

Simultaneously, the incident shock wave with velocity of u_0 also propagates to point *Q* in the same time interval. Thus, Eq. (16) can be rewritten as:

$$R_0\theta_w^* = (u_1 + a_1)\frac{R_0 \sin\theta_w^*}{u_0} \tag{17}$$

and the transition angle θ_w^* can be calculated by:

$$\frac{\sin\theta_w^*}{\theta_w^*} = \frac{u_0}{u_1 + a_1} \tag{18}$$

The previous research [17, 30-32] has proven that the θ_w^* predicted by Ben-Dor's model agrees well with the experiment results. However, the model still has its limitations that the effect of the radius R_0 is out of consideration, and it is inadequate to predict the triple-point trajectory of a strong shock wave. Moreover, for the ZND detonation model, the velocity u_1 and a_1 vary along the distance even behind the incident wave and hence, Ben-Dor's model cannot be applied directly to predict the θ_w^* of detonation wave reflection over a cylindrical concave wedge.

To further investigate the detonation reflection characteristics, the shock wave reflection under the Mach number of 5.4 was simulated as the reference case. Its reflection process is shown in Fig. 12. The triple-point trajectory for the shock wave reflection was recorded by tracking the density schlieren with constant time intervals, compared with the trajectory from the detonation Mach reflection under the same condition that is analyzed in Sect. 3.1 (the latter is referred to as the reference reactive case). The comparison of results are displayed in Fig. 13. The pressure curves in Fig. 13(a) show that for the reference reactive case, the dimensionless pressure p in the induction zone of detonation wave reaches 34.24, which is equal to that behind the shock front in the reference case. However, as the reaction step begins with heat release, the pressure of detonation decreases sharply in the reaction zone, and finally reaches 17.98 when the chemical reaction is completed. On the other hand, the comparison of the $H_m - \theta_w$ relation in Fig.

13(b) and the deviation ratio δ calculated by $\frac{H_{\text{m-ref.}}-H_{\text{m-ref.reactive}}}{H_{\text{m-ref.}}}$ in Fig. 13(c) indicate that the triple-point trajectories of detonation and inert shock wave are close and even coincide in a range of θ_w from 0° to 30°. For greater values of θ_w, a noticeable deviation can be observed and the H_m of reference reactive case is always shorter than that of reference case at the same θ_w position, resulting in a smaller transition angle θ_w^* for detonation reflection, and the deviation ratio δ also has the increase trend along with θ_w. The values of θ_w^* for the reference case and reference reactive case are 76.45° and 71.18°, respectively.

Although Ben-Dor's model cannot be used to predict the reflection of a detonation wave, the essence of the model can still be invoked to describe the mechanism of the similarities and differences between detonation and shock reflection. The model implies that the velocity of corner-generated signal u_s determines the reflection characteristics, which is mainly related to the flow and thermodynamic states behind the wave front. Sketches showing the variation of u_s in the reflection process are given in Fig. 14. For a detonation wave, the flow velocity u_1 in the induction zone is essentially equal to that behind the shock wave under the same Mach number. Therefore, when this region of detonation wave first propagates over the wedge, the corner signals generated by particles in the induction zone have an approximately equivalent value of u_s as with a planar shock wave (see Fig. 14(a)), thus resulting in a similar reflection trajectory at the beginning. Whereas the flow velocity u_1 decreases as the reaction zone and the region behind it (or the sonic plane) approach and sweep over the wedge tip afterward, leading to the attenuation of u_s, see Fig. 14(b). Consequently, the signal separates from the wave front earlier, which results a shorter length of Mach stem for the same θ_w and a smaller value of θ_w^*. The interpretation reveals a significant fact that the existence of the detonation thickness, i.e., the induction and reaction zones, plays a major role in determining how much the characteristics of detonation reflection differ from those of shock wave reflection.

3.3 Effects of various parameters on detonation reflection

It is shown that the finite reaction structure of a cellular detonation, i.e., with induction and reaction zones, plays a significant role in the reflection process. A parametric study was thus carried out to investigate the effect of various parameters which affect these two regions in detail. These parameters include the dimensionless activation energies ε_{I} and ε_{R}, CJ detonation Mach number M_{CJ}, the induction and reaction zone length ratio ϕ varied by the pre-exponential constants, and the curvature radius of the concave wedge R_0.

3.3.1 Effect of activation energies ε_{I} and ε_{R}

Considering that the activation energies ε_{I} and ε_{R} are mutually independent in the present two-step chemical kinetic model, their effects can be analyzed separately. In the simulations with various ε_{I}, ε_{I} was varied from 3 to 5.5 with an increment of 0.5, keeping the other parameters ε_{R} = 1, M_{CJ} = 5.4, and $R_0 =$ 750 the same. While in another group of simulations, ε_{R} was varied from 0.5 to 3 with an increment step of 0.5 for the same conditions of ε_{I} = 4, M_{CJ} = 5.4, and R_0 = 750. The parameters k_{I} and k_{R} were fixed for all these cases, with the value making the length ratio ϕ = 25 under the conditions of ε_{I} = 4, ε_{R} = 1 and M_{CJ} = 5.4. The resulting one-dimensional pressure curves, length ratio ϕ, and reflection parameters for the cases with various ε_{I} and ε_{R} are shown in Figs. 15 and 16, compared with the inert shock reflection results of the same incident Mach number.

Shown in Figs. 15(a) and 15(b), the change of ε_{I} has no influence on the state parameters of the steady ZND detonation as well as the induction and reaction zones based on the present chemical kinetic model. As a consequence, the $H_{\mathrm{m}}-\theta_{\mathrm{w}}$ relation curves are almost coincident with each other and the θ_{w}^{*} is essentially equal for all ε_{I} cases, see Figs. 15(c) and 15(d). These results imply that these cases with various ε_{I} have the same reflection characteristics, which means the change of ε_{I} has little effect on the reflection dynamics of the detonation wave. Compared with the cases with various ε_{I}, the variation of ε_{R} does not affect the induction zone, but the reaction zone length Δ_{R} as well as the length ratio ϕ are positively related with it, as shown in Figs. 16(a) and 16(b). The relation can be explained by Eq. (13) that the increase of ε_{R} reduces the reaction rate ω_{R} and extends the duration of the heat release reaction step, thus lengthening Δ_{R}. Differences can also be seen in the results of Figs. 16(c) and 16(d). Although the trajectories coincide with that of the shock wave at the early stage, the deviation becomes apparent as θ_{w} increases. The case with greater value of ε_{R} corresponds to longer H_{m} at the same θ_{w} position, and larger θ_{w}^{*} at the end.

3.3.2 Effect of CJ detonation Mach number M_{CJ}

The Mach number of the CJ detonation wave, M_{CJ} can affect the flow state in the induction and reaction zones directly. To examine its effect on the reflection process, simulations with various Mach number M_{CJ} were conducted. In the simulations, M_{CJ} ranged from 4.6 to 6.4 with an incremental step of 0.2, while the value of ϕ was fixed at $\phi = 25$ by adjusting the values of k_{I} and k_{R}. The other parameters are constant with $\varepsilon_{\mathrm{I}} = 4$, $\varepsilon_{\mathrm{R}} = 1$, and $R_0 = 750$. The shock wave reflection with each corresponding Mach number was also simulated. All the results are displayed in Fig. 17.

The pressure curve in Fig. 17(a) implies that varying M_{CJ} has a noticeable influence on the state properties behind the detonation and shock wave front. The peak pressure and the pressure after reaction completion rise evidently along with the increase of M_{CJ}. However, it can be observed from Figs.17(c) and 17(d) that both the trajectories of the reflection triple-point and the transition angles θ_{w}^{*} are almost independent of M_{CJ}. This equivalent reflection observation for strong shock waves with high Mach number has been verified by previous experimental research [46] and predicted by Ben-Dor's model [17, 30-32]. In addition, the reflection parameters of the detonation wave, i.e., H_{m} and θ_{w}^{*}, also converge when the length ratio ϕ of the detonation wave is kept constant, regardless of the varying flow state behind the wave front. This result is similar with the reflection characteristics of strong shock waves. Combining the analysis in Sect. 3.3.1, it can be confirmed that for stable cellular detonation waves with a relatively large Mach number, the flow state of a detonation wave has minimal influence on the reflection characteristics, whereas the critical parameters are the two length scales of the reaction structure, i.e., Δ_{I} and Δ_{R}, whose effect is represented by the length ratio ϕ in this study.

3.3.3 Effect of induction and reaction zone length ratio ϕ

As shown in the previous section, the length ratio ϕ is the key element in determining the reflection process of detonation waves. The effect of ϕ thus needs to be investigated in detail. In the present work, the rate constant was used as the means to vary ϕ. The change of k_{R} can modify this length ratio directly with little influence on the state parameters behind the wave.

The ϕ values varying from 10 to 30 with an interval of 5 were employed in the simulations. The other conditions are again ε_{I} = 4, ε_{R} = 1, M_{CJ} = 5.4, and R_0 = 750. The results are provided in Fig. 18. It can be observed that the pressure curve, H_{m} and θ_{w}^{*} variation with k_{R} presented in Fig. 18 are similar to that of various ε_{R} (see Fig. 16), i.e., the reflection parameters show positive relation with ϕ. Referring to the analysis in Sect. 3.2, this tendency can be interpreted as that the increase of ϕ, i.e., the elongation of Δ_{R}, delays the attenuation of signal velocity u_{s}. Hence, the corner-generated signals can propagate over a longer distance for the same duration of time. Consequently, the triple-point (as the extreme point where the signals can reach) can appear at a higher position on the incident wave, and the separation between the signals and the wave front is thus postponed.

From the above analysis, the length ratio ϕ has significant influence on the reflection characteristics of the detonation wave. To a certain extent, the detonation reflection parameters, H_{m} and θ_{w}^{*}, can be described by this length ratio. Any parameters in the reaction model that can change this length ratio ϕ will thus affect the reflection characteristics. Theoretically, at the limit when ϕ approaches infinity, the detonation will behave as a shock wave, so the limiting value of H_{m} and θ_{w}^{*} for detonation reflection is the value for shock wave reflection with the same Mach number.

3.3.4 Effect of wedge curvature radius R_0

The radius of wedge curvature R_0 does not belong to the parameters in the chemical reaction model, so it has no direct influence on the induction or reaction zone of the detonation wave. However, varying R_0 may change the transmission path or distance of the corner-generated signal, and in turn affect the reflection characteristics.

In the present research, R_0 values of 250 and 500 were applied to simulate the detonation reflection and corresponding shock reflection cases with various M_{CJ} as in Sect. 3.3.2. In addition, the R_0 values ranging from 250 to 1500 with an increment of 250 were chosen to simulate the detonation reflection cases with various ϕ as in Sect. 3.3.3. The numerical soot foils for some sample cases are given in Fig. 19, and the results of θ_{w}^{*} for all the cases are displayed in Fig. 20.

The results reveal that even for different R_0, the transition angles θ_{w}^{*} present similar variation regularities as a function of M_{CJ} or ϕ. The results further support the conclusion of the previous analysis that the length ratio ϕ is the key parameter in affecting the reflection characteristics of the detonation wave and has a positive correlation with the reflection parameters. Meanwhile, an evident tendency can be observed from Fig. 20(a) that the θ_{w}^{*} for both detonation and shock reflection decrease along with the increase of R_0. The variation trend for shock reflection has been confirmed by experiments [46], and Geva et al. [35] argued that the physical length scale which connects the triple-point and wedge tip is actually the curvature radius R_0, so the change of R_0 certainly will affect the reflection process. According to this interpretation, it is supposed that the θ_{w}^{*} for detonation reflection will have the similar trend to shock reflection under the effect of R_0. However, it is also observed in Fig. 20 that for a fixed M_{CJ} and ϕ, the variation of θ_{w}^{*} for detonation reflection is significantly greater than that for shock reflection with the same variation of R_0. This result suggests that there are some additional aspects leading to this trend deriving from the inherent characteristics of detonation waves.

To investigate the mechanism, the dimensionless height H_{m} / R_0 was calculated for the detonation reflection cases of ϕ = 10, 20, and 30 with R_0 from 250 to 1500. The $H_{\mathrm{m}}/R_0-\theta_{\mathrm{w}}$ relations and deviation ratio δ for few cases are displayed in Fig. 20. By comparing the relation curves in Figs. 21(a), 21(b) and 21(c), all the detonation reflection curves are coincident with the shock reflection curves at the beginning and then bifurcations appear at a certain curvature angle $\tilde{\theta}_{\mathrm{w}}$. The mechanism has been explained in Sect. 3.2 to be the variation of corner-generated signal velocity u_{s}. Moreover, it is noticed that for the same ϕ, the corresponding angle $\tilde{\theta}_{\mathrm{w}}$ of the bifurcation point reduces evidently as R_0 increases, and the trend can also be observed in the comparison of δ in Fig. 21(d).

Since the coincident part of the $H_{\mathrm{m}}/R_0-\theta_{\mathrm{w}}$ relation curves represents that the corner-generated signal velocity u_{s} for detonation reflection equals to that of inert shock reflection, it can be concluded that the detonation reflection process before the Mach stem reaches the bifurcation angle $\tilde{\theta}_{\mathrm{w}}$, corresponding to the coincident part of the curves, is actually controlled by the region in the ZND detonation structure which has the same flow velocity u_1 with that behind the shock front, i.e., the induction zone. Whereas the following reflection process with attenuated signal velocity of u_{s}, presenting as the bifurcation part of the curves, is controlled by the reaction zone and the region behind it (or the sonic plane). Since the induction zone lengths Δ_{I} of all cases are equivalent (equal to 1), it is reasonable to conjecture that for all the cases with various ϕ and R_0, the corner signals generated by the particles in the induction zone may travel an equivalent distance. According to the assumption in Ben-Dor's model that the corner-generated signals propagate along the wedge surface (see sect. 3.2), the travel distance $\tilde{S}$ of corner signals originated from the induction zone can be estimated by

$$\tilde{S}=R_0\tilde{\theta}_{\mathrm{w}} \tag{19}$$

To verify the conjecture, $\tilde{\theta}_{\mathrm{w}}$ was specified to be the corresponding angle of the last position where the deviation ratio $\delta \leq 3\%$. Thus the distance $\tilde{S}$ for various ϕ and R_0 was calculated and displayed in Fig. 22. Compared with Fig. 21, It is observed that although the angle $\tilde{\theta}_{\mathrm{w}}$ has significant variation for different R_0, the value of $\tilde{S}$ floats in a small range from 260 to 275, regardless of the variation of ϕ and R_0, which conforms to the conjecture.

By synthesizing the analysis above, the mechanism of the R_0 influence on the detonation reflection can be pinpointed. Since R_0 has no effect on the incident detonation wave, the structure of the induction and reaction zones is thus identical with various R_0 when the M_{CJ} and ϕ are fixed. Hence, the corner-generated signals controlled by the induction zone can propagate an approximately constant distance $\tilde{S}$ despite of different R_0, as shown in Fig. 22. However, if R_0 increases, the proportional influence and importance of this constant travel distance $\tilde{S}$, which is controlled by the corner signals originating from the induction zone, decreases relative to the entire reflection distance. Relatively, in a larger part of the reflection process, the signals are generated by the particles behind the induction zone and persist in a state with the minimum velocity, which eventually makes the signal separate from the wave front earlier with a smaller transition angle θ_{w}^{*}, as presented in Fig. 20.

4. Conclusions

The reflection of stable cellular detonation waves with regular cellular patterns over a cylindrical concave wedge was investigated through two-dimensional numerical simulations by solving the reactive Euler equations with a two-step induction-reaction kinetic model using the adaptive mesh refinement code AMROC. The detonation reflection dynamics and its characteristics were studied and compared with that of a planar shock wave, and the mechanism was discussed by adopting the length-scale concept. The effects of various parameters on the reflection were also investigated in detail.

Similar to the planar shock wave case, the stable cellular detonation reflection process also experiences the transition between various reflection types of DiMR-StMR-InMR-TRR. In the lower angle θ_w area near the wedge tip, the triple-point trajectory of detonation and shock reflection coincide with each other for the same Mach number of the leading wave front. As θ_w increases, the triple-point trajectory of detonation Mach reflection deviates from that of the shock reflection with a reduced Mach stem height H_m and terminates at a smaller MR-RR transition angle θ_w^*. The mechanism governing the reflection type and transition is discussed by considering the velocity variation of corner signals generated by fluid particles behind the detonation wave front around the wedge tip. Since the flow velocity in the induction zone is the same as that behind a shock wave of the same Mach number, the corner-generated signal velocity u_s is essentially equivalent with that of a shock wave when the induction zone first propagates over the wedge tip, making the reflection behavior similar to the shock reflection. However, the signal velocity u_s gradually attenuates as the reaction zone and the region behind the sonic locus approach and sweep over the tip, which results in reducing the H_m and θ_w^* afterward.

It can be suggested that for stable cellular detonation waves, the flow state of detonation has almost no direct influence on the reflection process. The key parameters appear to be the induction and reaction zone length ratio ϕ, which can be regarded as an indicator in evaluating the reflection characteristics of the detonation wave. The presence of the finite reaction structure for a detonation wave and all the effects resulting from different chemical reaction parameters on the reflection characteristics can be synthesized into the effect of ϕ. The ratio ϕ has a positive correlation with the reflection parameters H_m and θ_w^*.

Lastly, the variation of wedge curvature radius R_0 has no direct influence on the structure of detonation wave, and hence the initial corner-generated signals controlled by the flow particles in the induction zone can propagate a nearly constant distance $\tilde{S}$ despite various values of R_0. Nevertheless, the increase of R_0 makes the proportion of this distance $\tilde{S}$ resulting from the induction-based signals decrease relative to the entire reflection distance, and in addition expands the region where the corner signals can only be generated by particles behind the induction zone, so the corner signals persist in a state with the minimum velocity, which induces lower H_m and terminating the Mach reflection with decreasing θ_w^*.

Acknowledgements

This work is supported by the National Natural Science Foundation of China under Grant No. 91441201 and No. 51476186 and the Natural Sciences and Engineering Research Council of Canada (NSERC) (No. RGPIN-2017-06698). The authors thank A. J. Higgins for comments and feedback on the manuscript.

Reference

[1] P. Wolanski, Detonative propulsion, Proc. Combust. Inst. 34 (1) (2013) 125–158.

[2] F.K. Lu, E. Braun, Rotating detonation wave propulsion: Experimental challenges, modeling, and engine concepts, J. Propul. Power 30 (5) (2014) 1125–1142.

[3] R.W. Houim, R.T. Fievisohn, The influence of acoustic impedance on gaseous layered detonations bounded by an inert gas, Combust. Flame 179 (2017) 185-198.

[4] M. Reynaud, F. Virot, A. Chinnayya, A computational study of the interaction of gaseous detonations with a compressible layer, Phys. Fluids 29 (5) (2017) 056101.

[5] Y. Kudo, Y. Nagura, J. Kasahara, Y. Sasamoto, A. Matsuo, Oblique detonation waves stabilized in rectangular-cross-section bent tubes, Proc. Combust. Inst. 33 (2011) 2319-2326.

[6] H. Nakayama, T. Moriya, J. Kasahara, A. Matsuo, Y. Sasamoto, I. Funaki, Stable detonation wave propagation in rectangular-cross-section curved channels, Combust. Flame 159 (2012) 859-869.

[7] H. Nakayama, J. Kasahara, A. Matsuo, I. Funaki, Front shock behavior of stable curved detonation waves in rectangular-cross-section curved channels, Proc. Combust. Inst. 34 (2013) 1939-1947.

[8] Y. Sugiyama, Y. Nakayama, A. Matsuo, H. Nakayama, J. Kasahara, Numerical Investigations on Detonation Propagation in a Two-Dimensional Curved Channel, Combust. Sci. Tech. 186 (2014) 1662-1679.

[9] J. Li, J. Ning, H. Zhao, L. Hao, C. Wang, Numerical Investigation on the Propagation Mechanism of Steady Cellular Detonations in Curved Channels, Chin. Phys. Lett. 32 (4) (2015) 048202.

[10] X. Yuan, J. Zhou, Z. Lin, X. Cai, Adaptive simulations of detonation propagation in 90-degree bent tubes, Int. J. Hydrogen. Energy 41 (2016) 18259-18272.

[11] Z. Xia, H. Ma, C. Zhuo, C, Zhou, Propagation process of H_2/air rotating detonation wave and influence factors in plane-radial structure, Int. J. Hydrogen. Energy 43 (2018) 4609-4622.

[12] M. Short, C. Chiquete, J.J. Quirk, Propagation of a stable gaseous detonation in a circular arc configuration, Proc. Combust. Inst. 000 (2018) 1-8.

[13] R. Ong, On the interaction of a Chapman-Jouguet detonation wave with a wedge, University of Michigan, Ann Arbor, MI, 1955.

[14] R. Akbar, Mach reflection of gaseous detonations, Rensselaer Polytechnic Institute, Troy, NY, 1997.

[15] H. Li, G. Ben-Dor, H. Grönig, Analytical study of the oblique reflection of detonation waves, AIAA J. 35 (1997) 1712–1720.

[16] J. von Neumann, Collected works, vol. 6, Pergamon, Oxford, UK, 1961.

[17] G. Ben-Dor, Shock wave reflection phenomena, 2nd ed., Springer-Verlag, New York, US, 2007.

[18] W. Chester, CXLV. The quasi-cylindrical shock tube, Philos. Mag. 45 (1954) 1293–1301.

[19] R.F. Chisnell, The motion of a shock wave in a channel, with applications to cylindrical and spherical shock waves, J. Fluid Mech. 2 (1957) 286–298.

[20] G.B. Whitham, A new approach to problems of shock dynamics. Part 1. Two-dimensional problems, J. Fluid Mech. 2 (1957) 146–171.

[21] A.V. Trotsyuk, Numerical study of the reflection of detonation waves from a wedge, Combust. Explos. Shock Waves 35 (1999) 690–697.

[22] G.O. Thomas, R.L. Williams, Detonation interaction with wedges and bends, Shock Waves 11 (2002) 481–492.

[23]J. Shepherd, E. Schultz, R. Akbar, Detonation diffraction, 22nd International Col- loquium on the Dynamics of Explosions and Reactive Systems, Imperial College, London, 1999.

[24] Y. Fortin, J. Liu , J.H.S. Lee , Mach reflection of cellular detonations, Combust. Flame 162 (2015) 819–824 .

[25] J. Li, J. Ning, J.H.S. Lee , Mach reflection of a ZND detonation wave, Shock Waves 25 (2015) 293–304 .

[26] J. Li, J.H.S. Lee, Numerical simulation of Mach reflection of cellular detonations, Shock Waves 26 (2016) 1–10.

[27] J. Li, H. Ren, X. Wang, J. Ning, Length scale effect on Mach reflection of cellular detonations, Combust. Flame 189 (2018) 378–392.

[28] H. G. Hornung, H. Oertel, R. J. Sandeman, Transition to Mach reflexion of shock waves in steady and pseudosteady flow with and without relaxation, J. Fluid Mech. 90 (1979) 541-560.

[29] S. Itoh, N. Okazaki, M. Itaya, On the transition between regular and Mach reflection in truly non-stationary flows, J. Fluid Mech. 108 (1981) 383-400.

[30] G. Ben-Dor, K. Takayama, Analytical prediction of the transition from Mach to regular reflection over cylindrical concave wedges, J. Fluid Mech. 158 (1985) 365-380.

[31] G. Ben-Dor, K. Takayama, J. M. Dewey, Further analytical considerations of weak planar shock wave reflections over a concave wedge, Fluid Dyn. Res. 2 (1987) 77-85.

[32] K. Takayama, G. Ben-Dor, A reconsideration of the transition criterion from Mach to regular reflection over cylindrical concave surfaces, KSME J. 3 (1989) 6-9.

[33] S. Gruber, Weak shock wave reflections from concave curved surfaces, Master Thesis, University of the Witwatersrand, ZA, 2012.

[34] B. Skews, A. Blitterswijk, Shock wave reflection off coupled surface, Shock Waves 21 (2011) 491–498.

[35] M. Geva, O. Ram, O. Sadot, The non-stationary hysteresis phenomenon in shock wave reflections, J. Fluid Mech. 732 (2013) R1.

[36] O. Ram, M. Geva, O. Sadot, High spatial and temporal resolution study of shock wave reflection over a coupled convex–concave cylindrical surface, J. Fluid Mech. 768 (2015) 219–239.

[37] V. Soni, O. Roussel, A. Hadjadj, On the accuracy and efficiency of point-value multiresolution algorithms for solving scalar wave and Euler equations, J. Comput. Appl. Maths 323 (2017) 159-175.

[38] S.S.M. Lau- Chapdelaine, M.I. Radulescu, Viscous solution of the triple-shock reflection problem, Shock Waves 26 (2016) 551-560.

[39] C.M. Romick, T.D. Aslam, M. Powers, The effect of diffusion on the dynamics of unsteady detonations. J. Fluid Mech. 699 (2012) 453-464.

[40] K. Mazaheri, Y. Mahmoudi, M.I. Radulescu, Diffusion and hydrodynamic instabilities in gaseous detonations. Combust. Flame 159(6) (2012) 2138-2154.

[41] M.I. Radulescu, A detonation paradox: Why inviscid detonation simulations predict the incorrect trend for the role of instability in gaseous cellular detonations? Combust. Flame 195 (2018) 151-162.

[42] H.D. Ng, M.I. Radulescu, A.J. Higgins, N. Nikiforakis, J.H.S. Lee, Numerical investigation of the instability for onedimensional Chapman–Jouguet detonations with chain-branching kinetics, Combust. Theor. Model. 9 (3) (2005) 385-401.

[43] R. Deiterding, Parallel adaptive simulation of multidimensional detonation structures. PhD Thesis, Brandenburgische Technische Universität Cottbus, DE, 2003.

[44] E. Hairer, G. Wanner, Solving ordinary differential equations II: stiff and differential-algebraic problems. 2nd ed. Springer-Verlag, Berlin, DE, 1996.

[45] R.P. Fedkiw, A non-oscillatory Eulerian approach to interfaces in multimaterial flows (the ghost fluid method), J. Comput. Phys. 152 (1999) 457-492.

[46] K. Takayama, M. Sasaki, Effects of radius of curvature and initial angle on the shock transition over concave and convex walls, Rep. Inst. High Speed Mech. 46 (1983) 1–30.

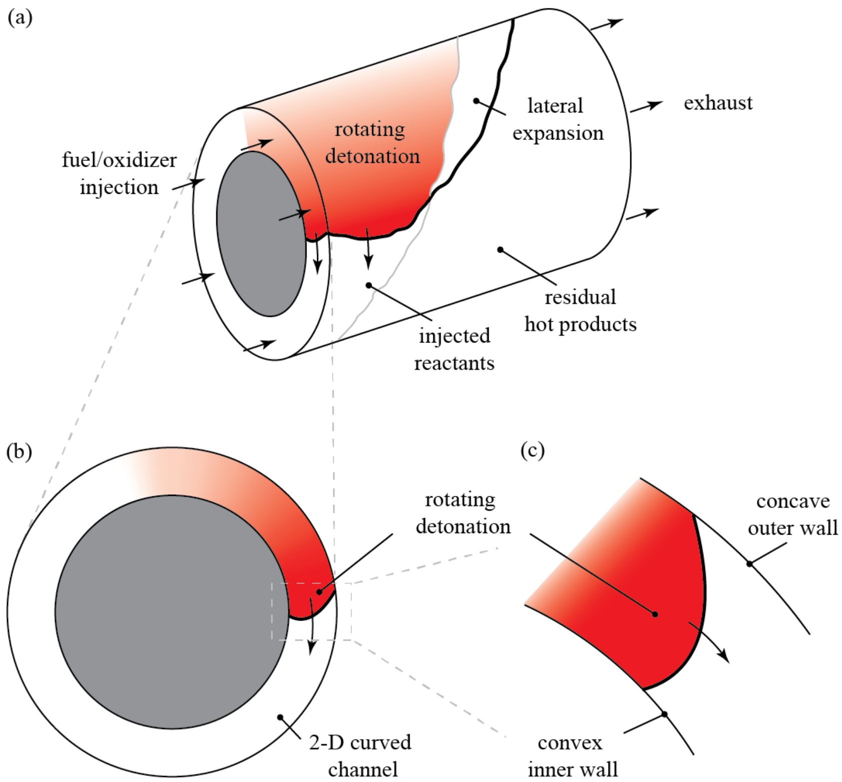

Figure 1: Conceptual illustration of (a) the combustion chamber of a rotating detonation engine (RDE), (b) detonation propagation in a two-dimensional curved channel, and (c) a detonation wave bounded by a convex inner wall and a concave outer wall.

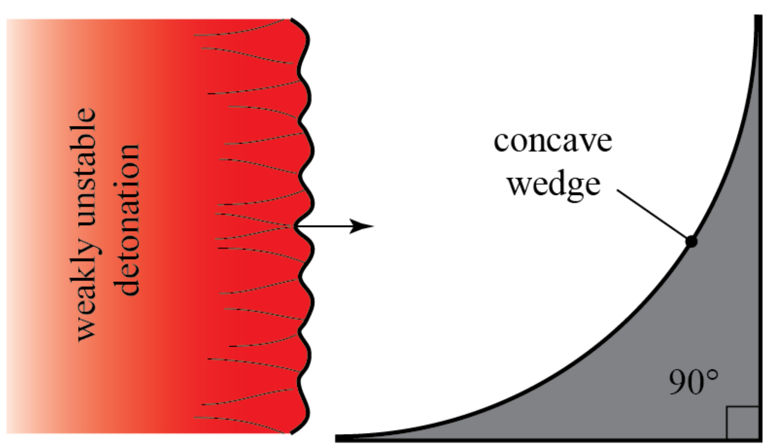

Figure 2: Illustration of the problem under consideration—the reflection of a weakly cellular detonation wave over a 90° concave wedge.

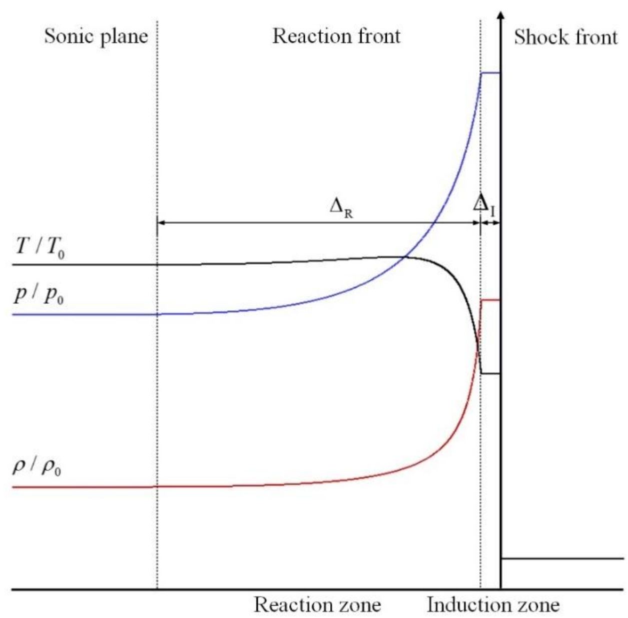

Figure 3: A sketch of the ZND detonation wave structure formed by the two-step induction-reaction model.

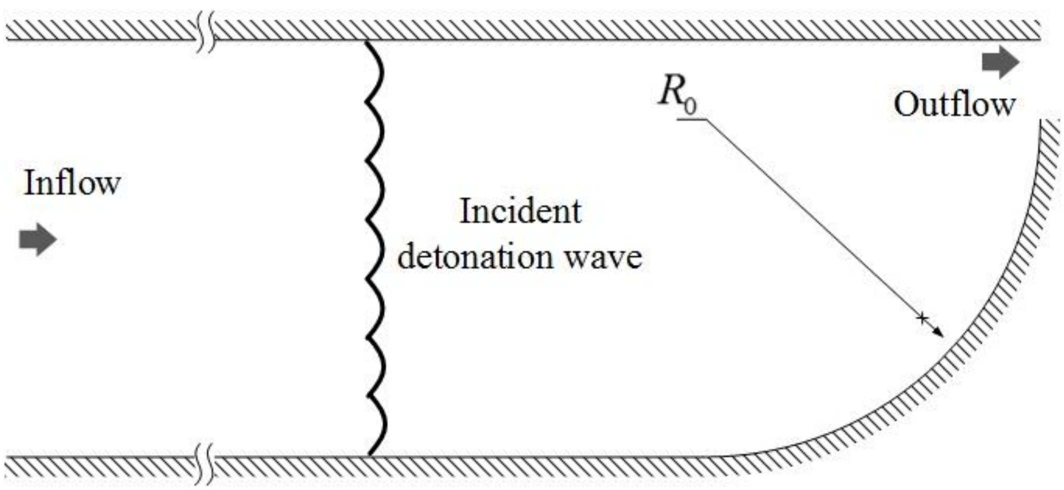

Figure 4: Schematic of the computational domain.

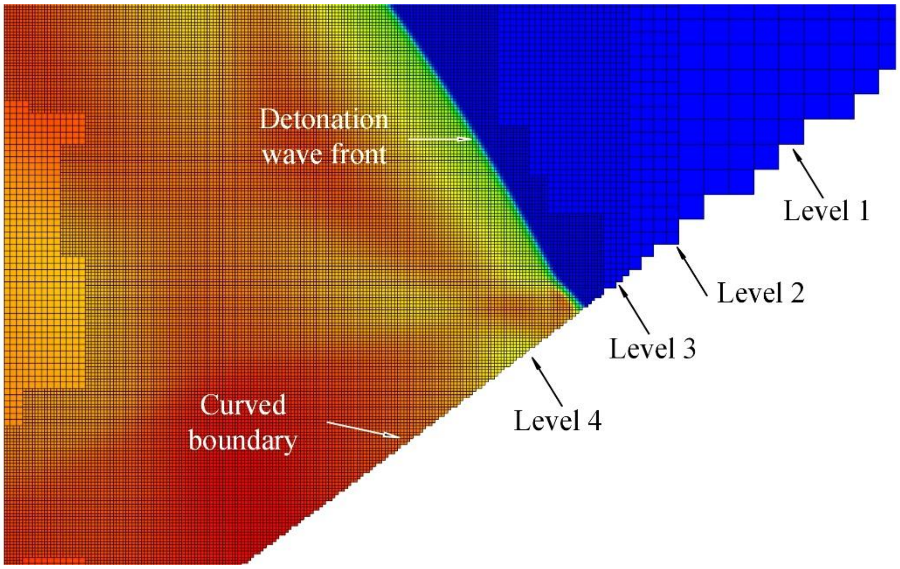

Figure 5: Grid distribution near the wall with four levels of resolution refinement.

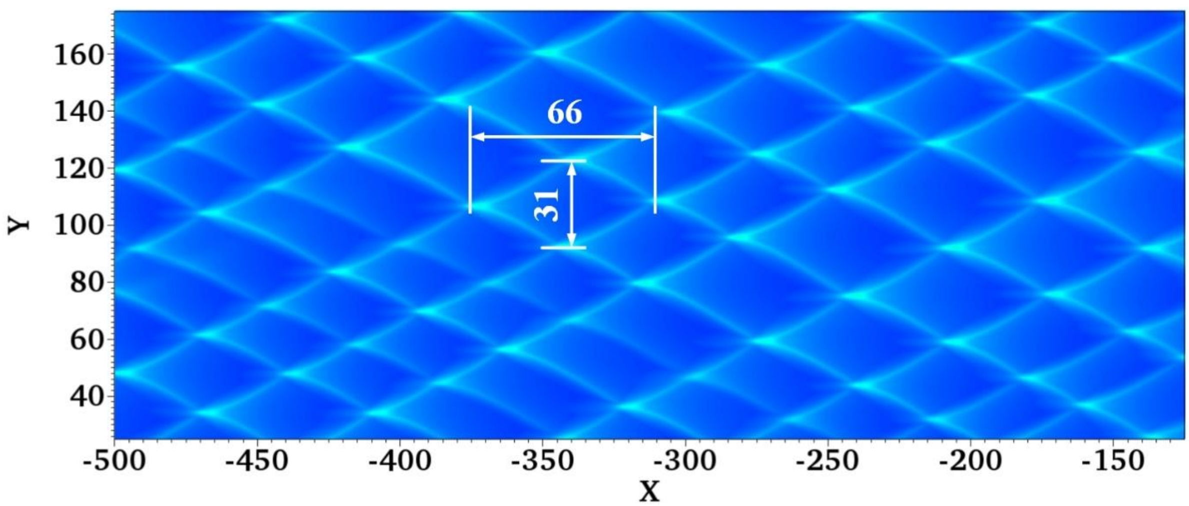

Figure 6: Numerical soot foil developed by the incident detonation wave.

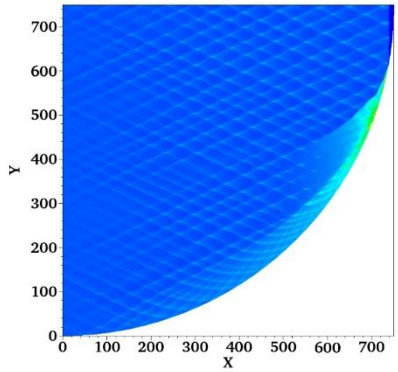

(a) $\Delta x_{\text{min}} = 16$ pts/Δ_{I}

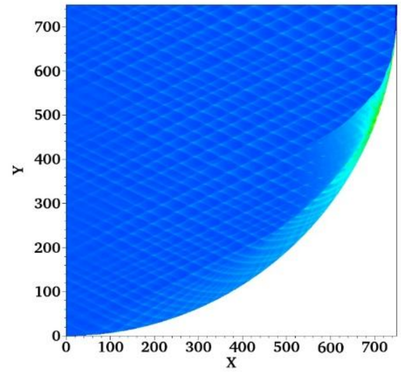

(b) $\Delta x_{\text{min}} = 32$ pts/Δ_{I}

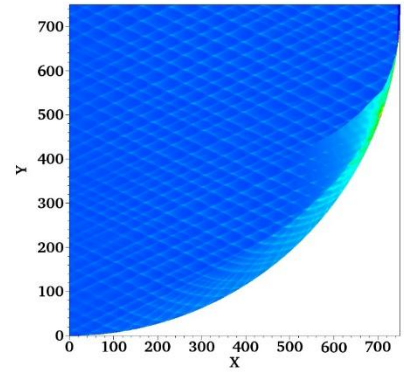

(c) $\Delta x_{\text{min}} = 64$ pts/Δ_{I}

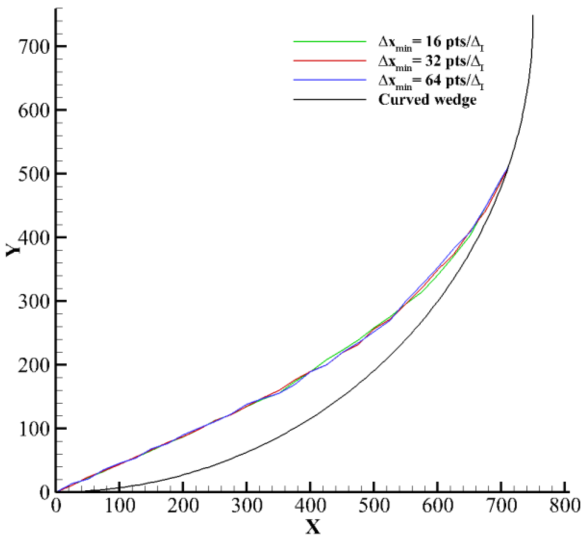

(d) Trajectories of reflection triple-point

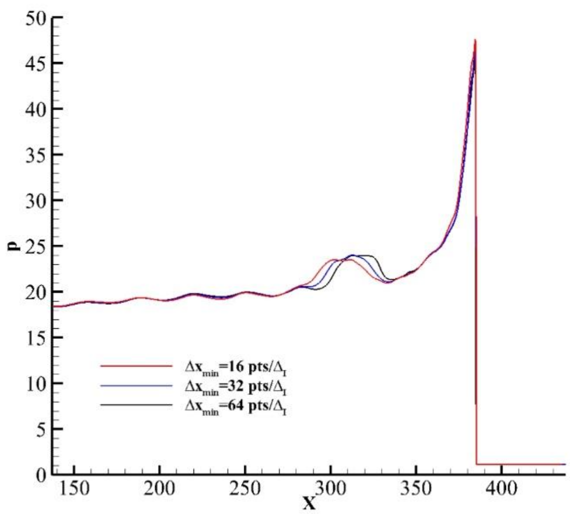

(e) Pressure curves along the fixed height of y = 140 at the same time instant.

Figure 7: Numerical soot foils, trajectories of Mach reflection triple-point and pressure curve for three different mesh resolutions.

Table 1: The transition angle θ_{w}^{*} and CPU time for three different mesh resolutions.

Resolution	$\Delta x_{\text{min}} = 16$ pts/Δ_{I}	$\Delta x_{\text{min}} = 32$ pts/Δ_{I}	$\Delta x_{\text{min}} = 64$ pts/Δ_{I}
θ_{w}^{*} (°)	71.38	71.18	71.04
CPU time (s)	15341	31697	64934

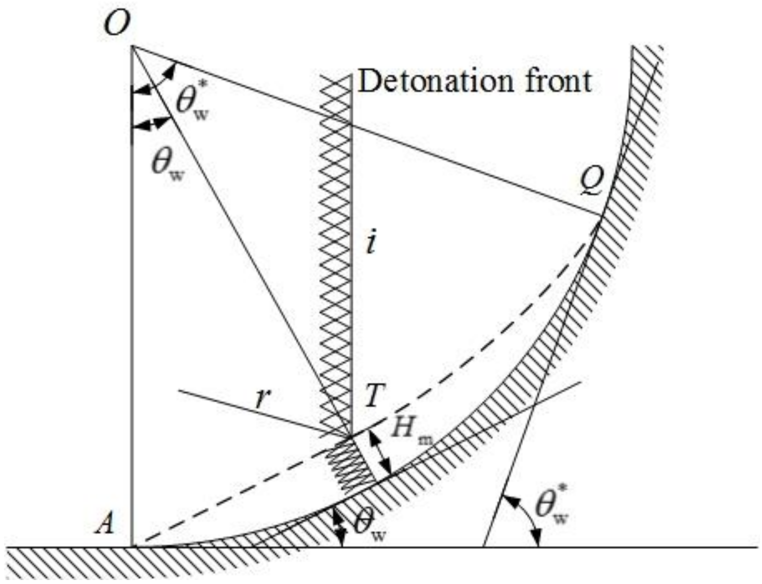

Figure 8: A sketch of the detonation wave reflection process over cylindrical concave wedge: *A*, wedge tip; *O*, center of curvature of wedge, *Q*, MR-RR transition position; *T*, Mach reflection triple-point; θ_{w}^{*}, transition angle; θ_{w}, position angle of *T*; H_{m}, vertical height from *T* to wedge surface; *i*, incident wave; *r*, reflected wave; dashed line, trajectory of reflection triple-point.

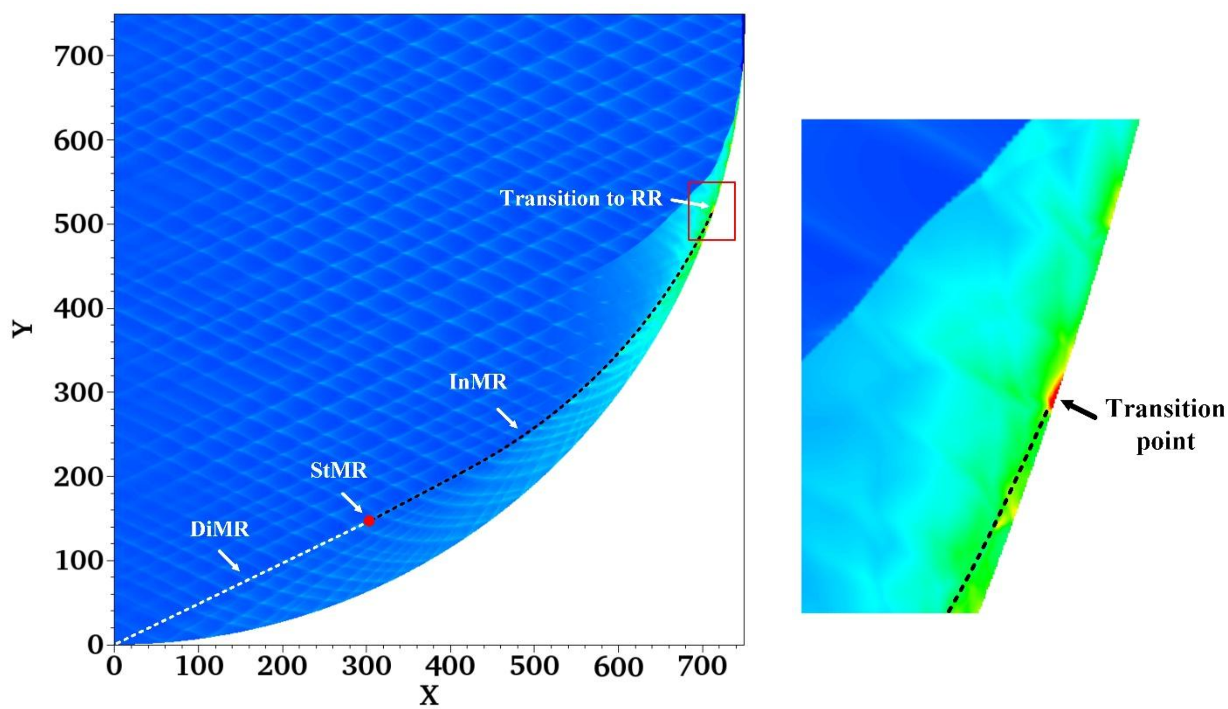

Figure 9: Numerical soot foils of detonation wave reflection presenting the transition of reflection types and the enlarged view around the point of MR-RR transition (dotted line: trajectory of reflection triple-point).

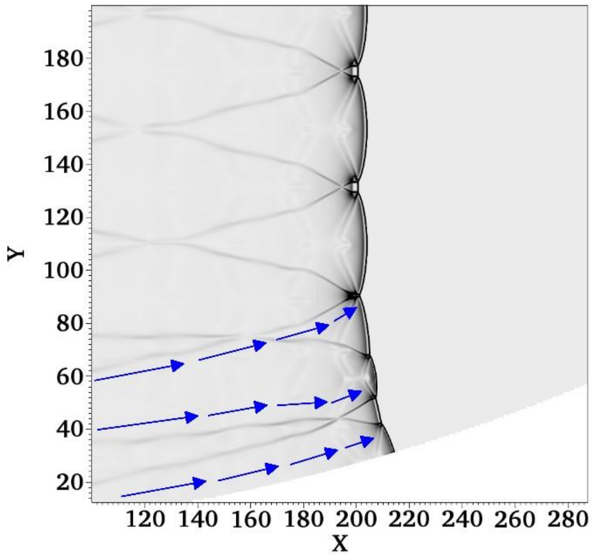

(a) Direct-Mach reflection (DiMR)

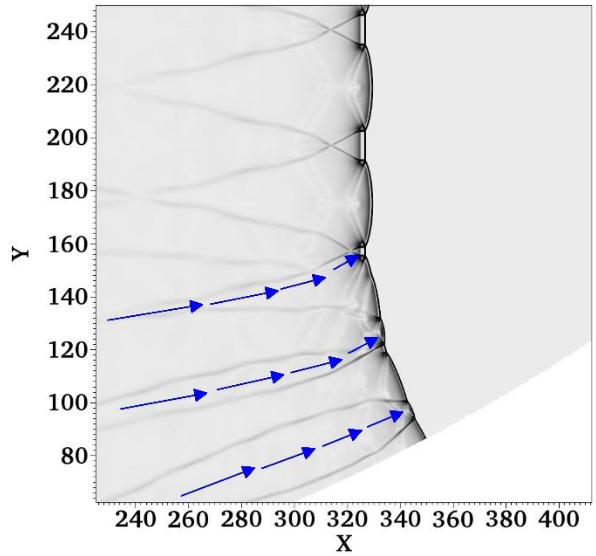

(b) Stationary-Mach reflection (StMR)

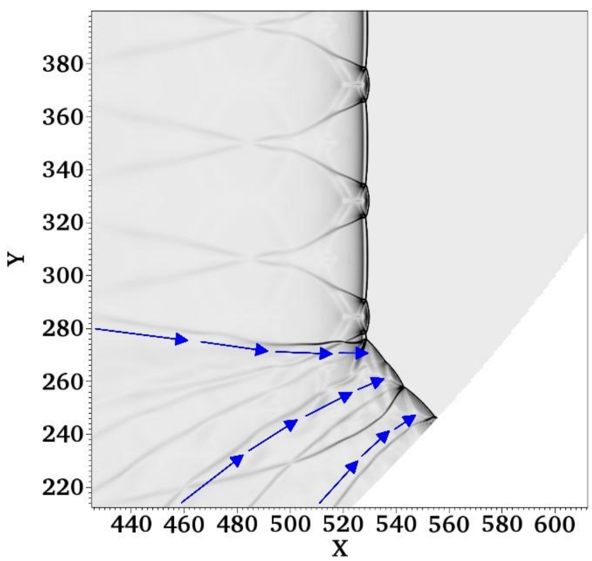

(c) Inverse-Mach reflection (InMR)

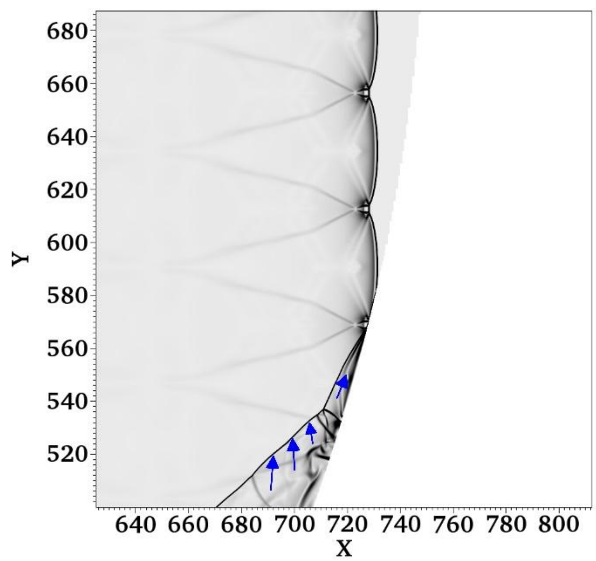

(d) Transitioned regular reflection (TRR)

Figure 10: Overlays of density schlieren and flow vector presenting the structure of detonation wave under different reflection types.

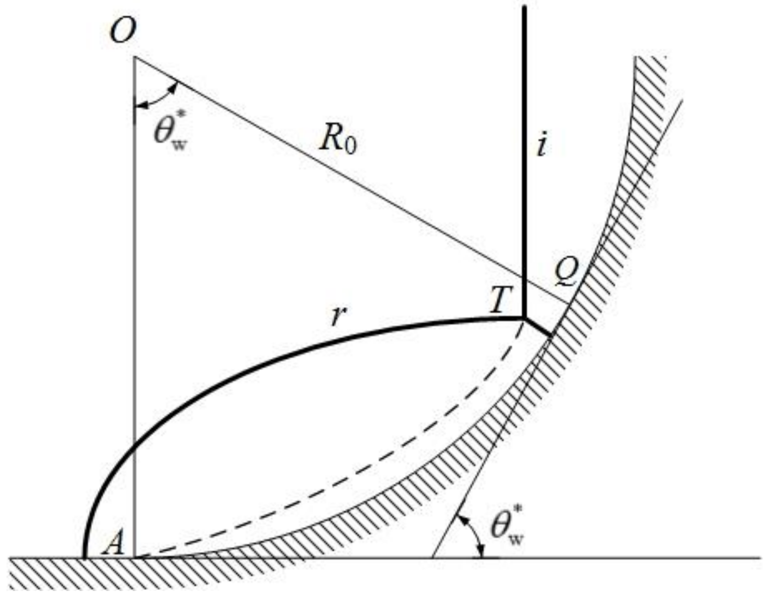

Figure 11: A sketch of calculation model of θ_w^* for shock wave reflection: *A*, wedge tip; *O*, center of curvature of wedge; *Q*, MR-RR transition position; *T*, Mach reflection triple-point; R_0, radius of wedge curvature; θ_w^*, transition angle; *i*, incident wave; *r*, reflected wave; dashed line, propagation path of corner-generated signals.

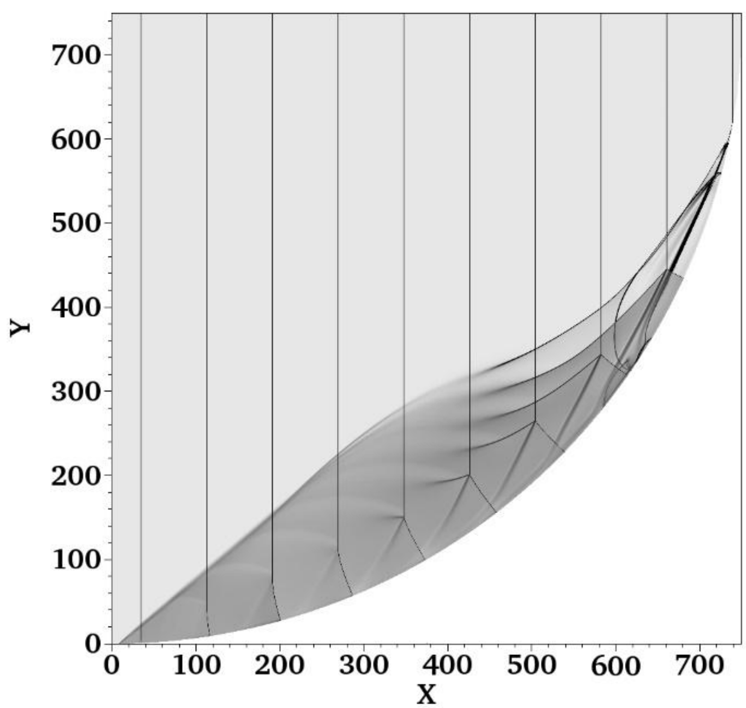

Figure 12: Density schlieren overlays of shock wave reflection process.

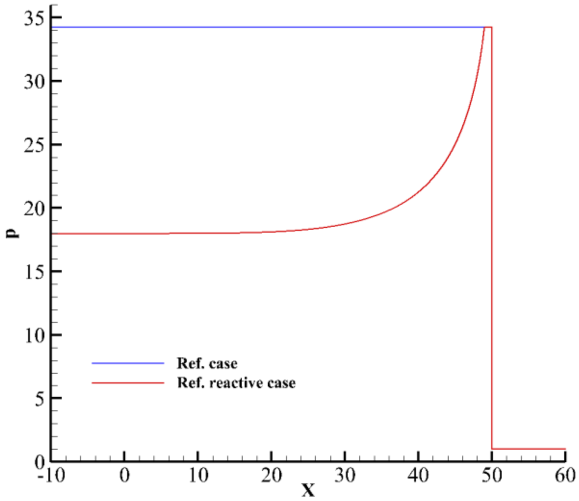

(a) One-dimensional pressure curve

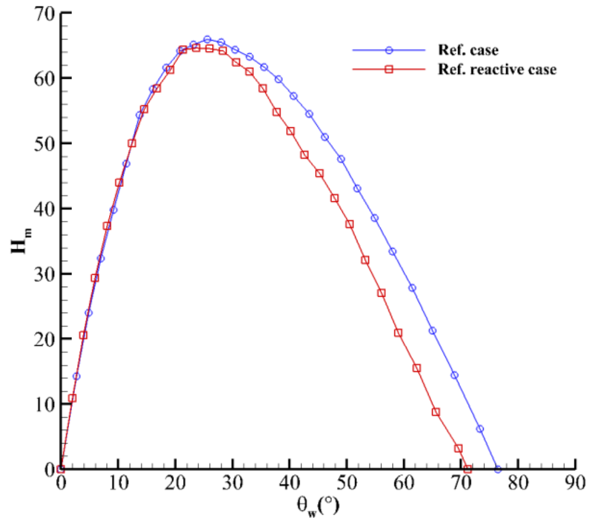

(b) $H_{\mathrm{m}}-\theta_{\mathrm{w}}$ relation

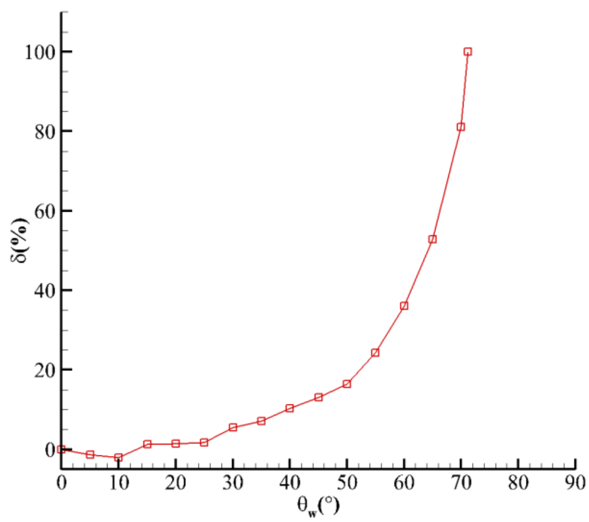

(c) Deviation ratio δ for H_{m}

Figure 13: Comparison of reflection characteristics for detonation and shock waves.

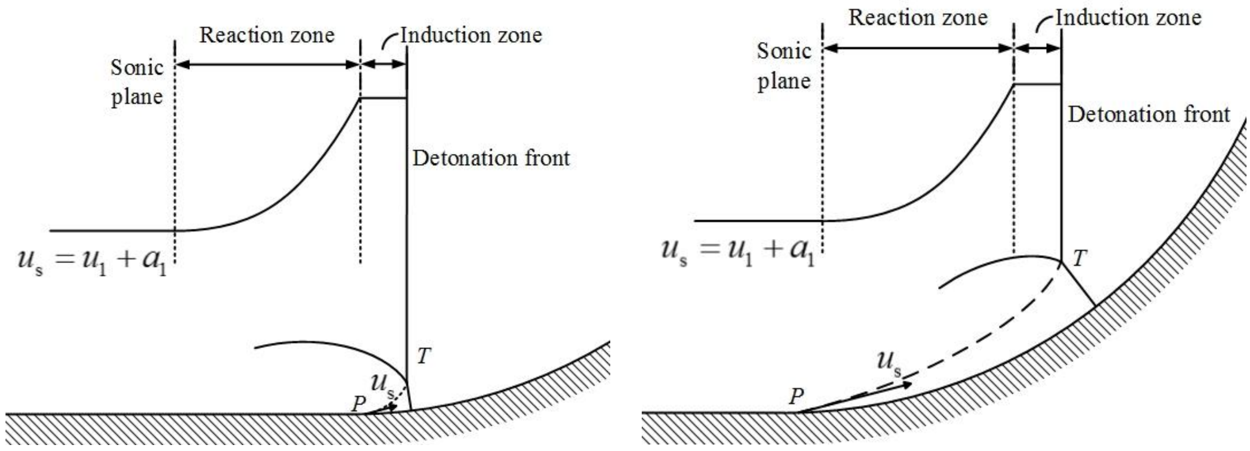

(a) Detonation wave first propagates through the wedge tip

(b) The finite reaction zone (sonic plane) reaches the wedge tip

Figure 14: Sketches of the variation of u_s in the detonation wave reflection process: *P*, position of the fluid particle; *T*, Mach reflection triple-point.

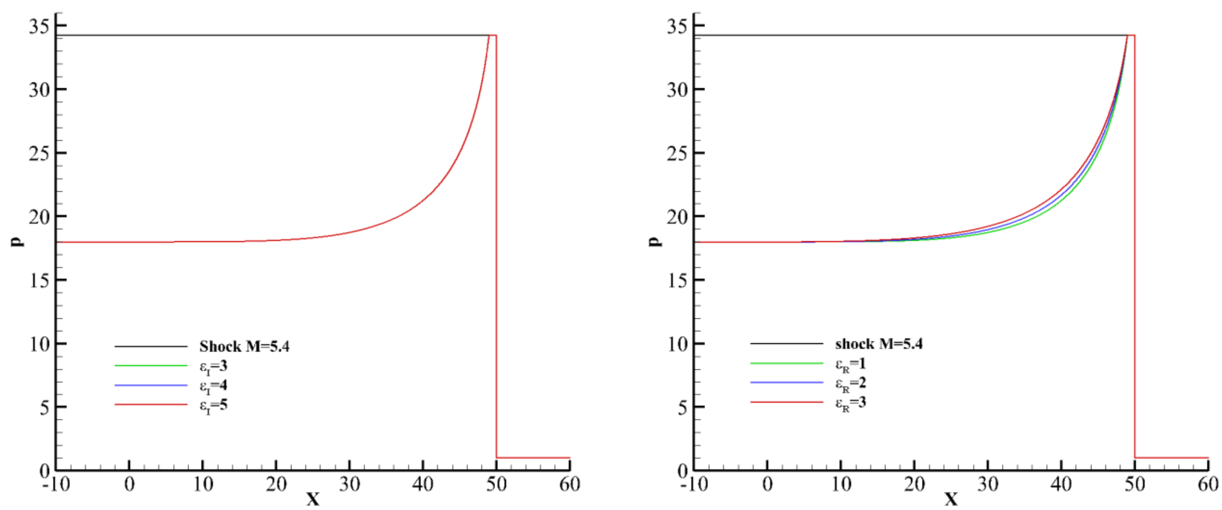

(a) One-dimensional pressure curve

(a) One-dimensional pressure curve

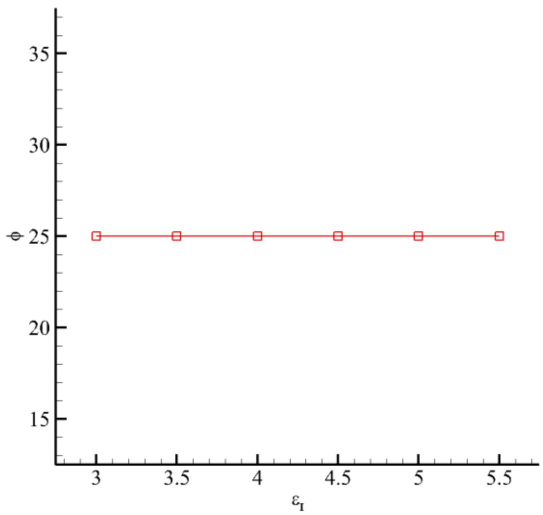

(b) $\phi - \varepsilon_{\mathrm{I}}$ relation

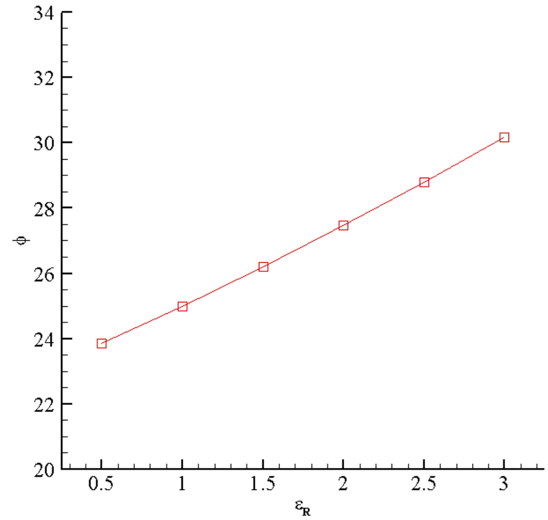

(b) $\phi - \varepsilon_{\mathrm{R}}$ relation

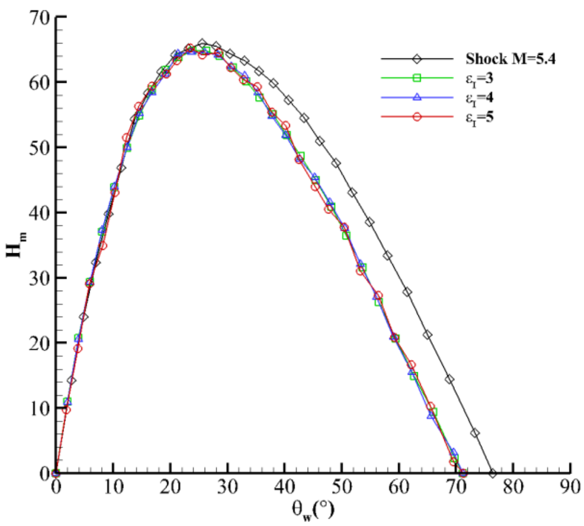

(c) $H_{\mathrm{m}} - \theta_{\mathrm{w}}$ relation

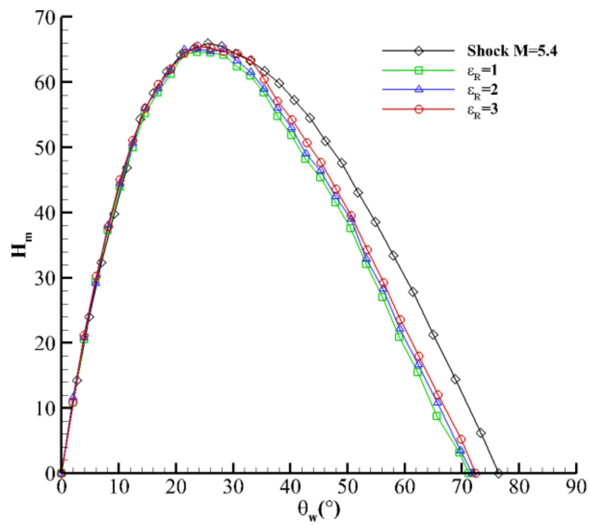

(c) $H_{\mathrm{m}} - \theta_{\mathrm{w}}$ relation

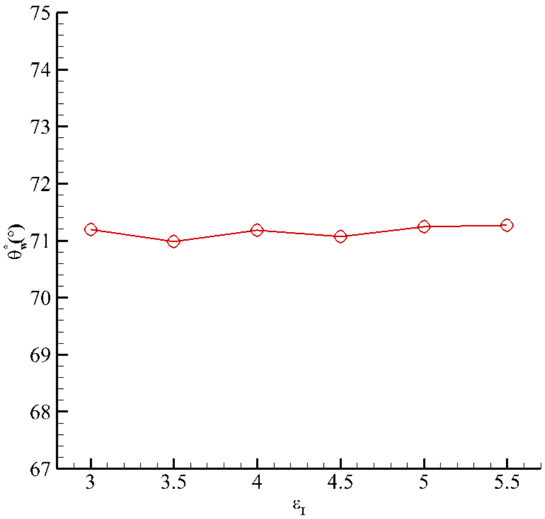

(d) $\theta_{\mathrm{w}}^{*} - \varepsilon_{\mathrm{I}}$ relation

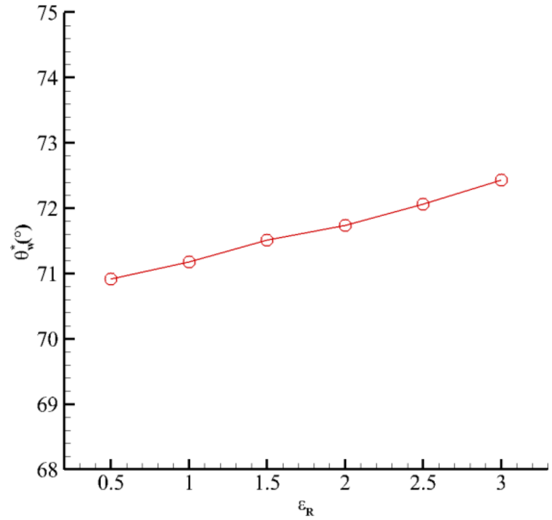

(d) $\theta_{\mathrm{w}}^{*} - \varepsilon_{\mathrm{R}}$ relation

Figure 15: Parameters for detonation reflection with various ε_{I}.

Figure 16: Parameters for detonation reflection with various ε_{R}.

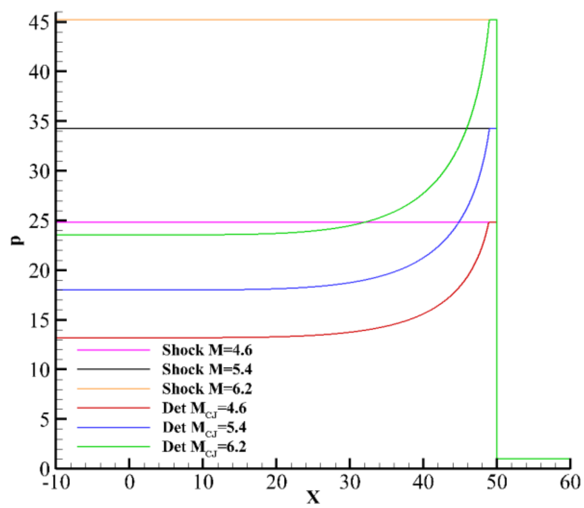

(a) One-dimensional pressure curve

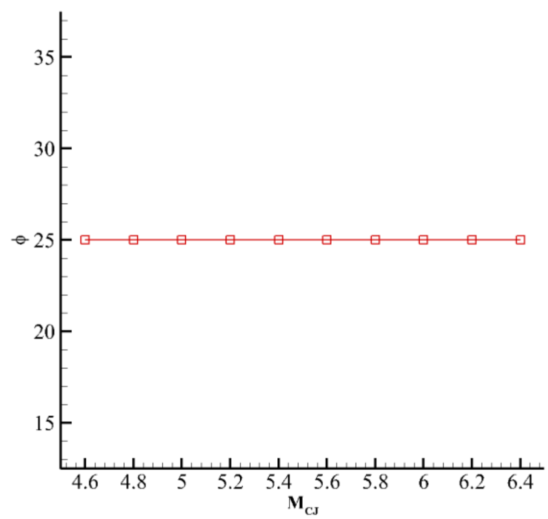

(b) $\phi - M_{\mathrm{CJ}}$ relation

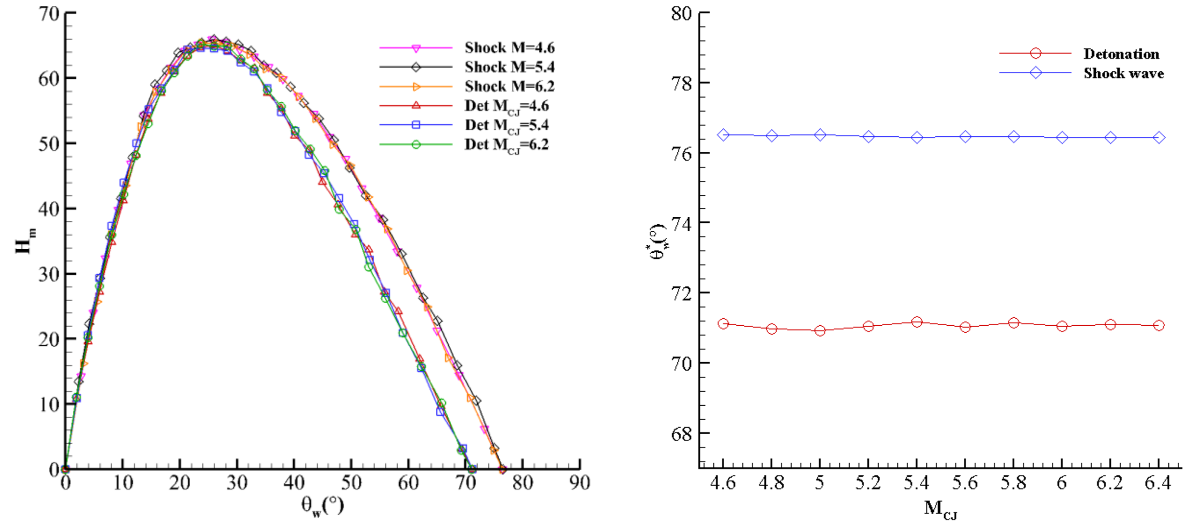

(c) $H_m - \theta_w$ relation (d) $\theta_w^* - M_{CJ}$ relation

Figure 17: Parameters for detonation reflection with various M_{CJ}.

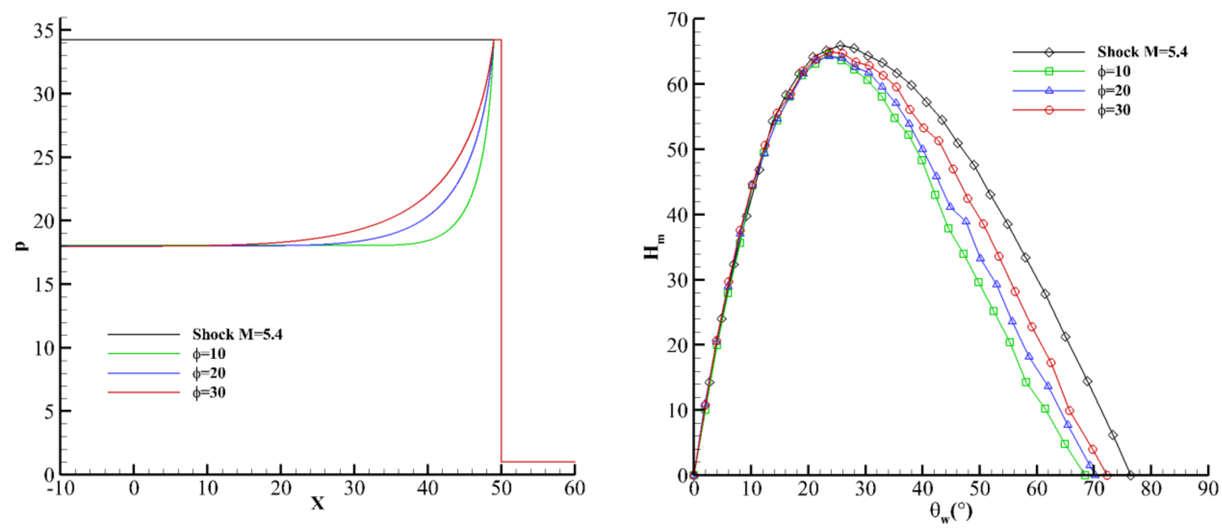

(a) One-dimensional pressure curve (b) $H_m - \theta_w$ relation

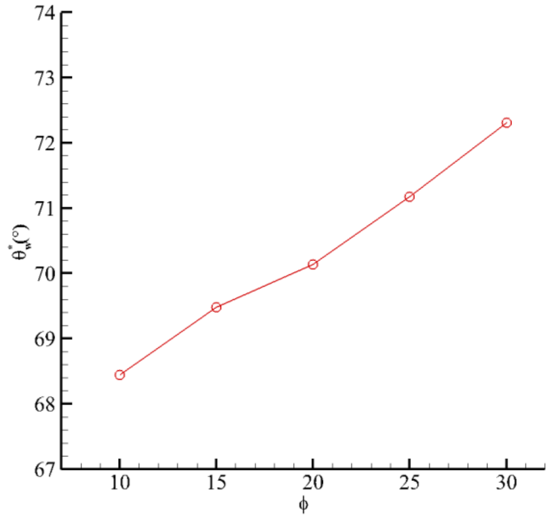

(c) $\theta_{\mathrm{w}}^{*} - \phi$ relation

Figure 18: Parameters for detonation reflection with various ϕ .

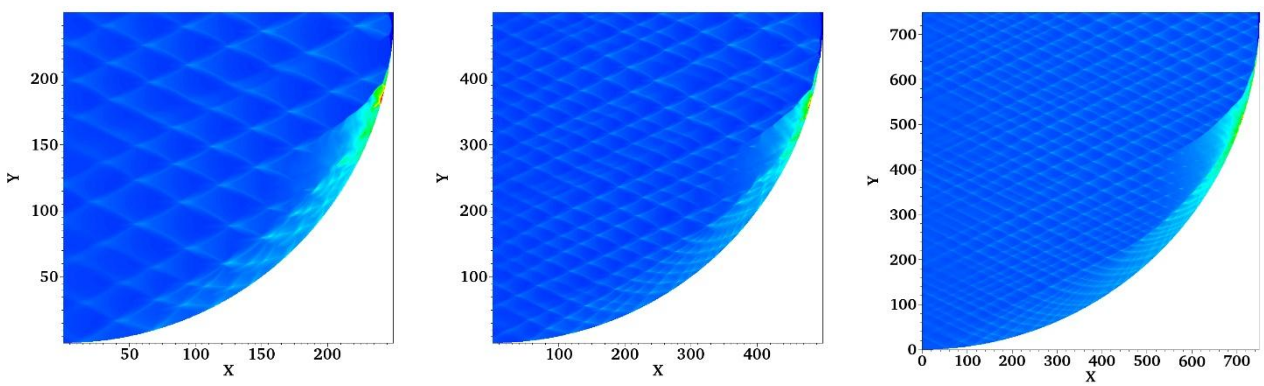

(a) R_0 = 250 (b) R_0 = 500 (c) R_0 = 750

Figure 19: Numerical soot foils for detonation wave reflection with various R_0 .
(ε_{I} = 4, ε_{R} = 1, M_{CJ} = 5.4, and ϕ = 25)

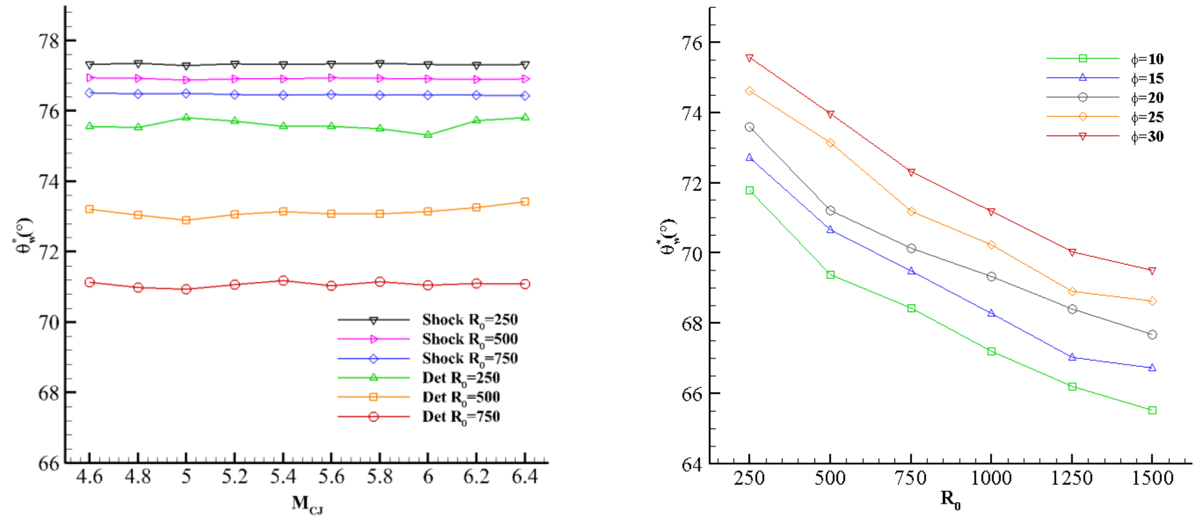

(a) $\theta_{\mathrm{w}}^{*} - M_{\mathrm{CJ}}$ relation with $\phi = 25$ (b) $\theta_{\mathrm{w}}^{*} - R_{0}$ relation with various ϕ

Figure 20: Transition angle θ_{w}^{*} for different cases with various R_0.

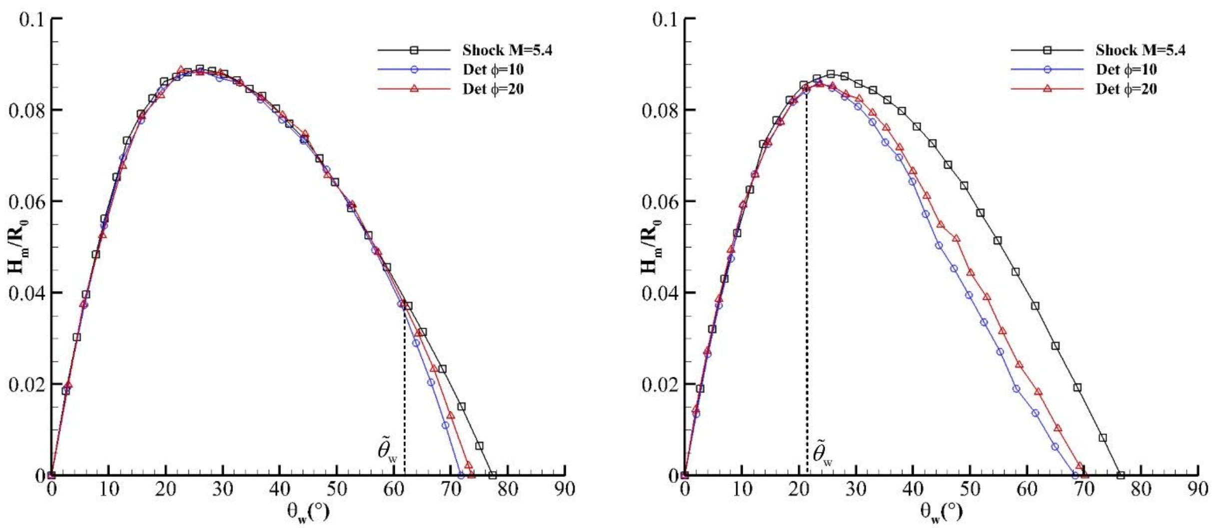

(a) $H_{\mathrm{m}} / R_0 - \theta_{\mathrm{w}}$ relation with $R_0 = 250$ (b) $H_{\mathrm{m}} / R_0 - \theta_{\mathrm{w}}$ relation with $R_0 = 750$

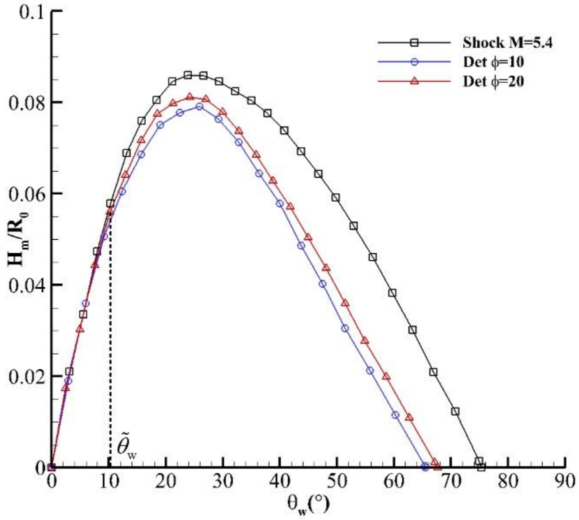

(c) $H_\mathrm{m} / R_0 - \theta_\mathrm{w}$ relation with $R_0 = 1500$

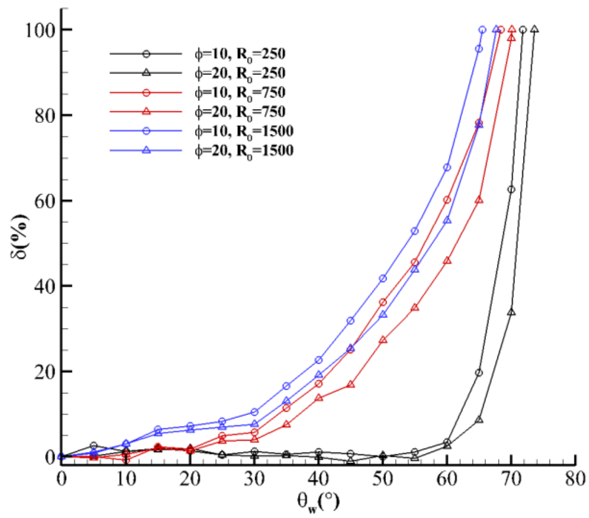

(d) Deviation ratio δ for each case

Figure 21: $H_\mathrm{m} / R_0 - \theta_\mathrm{w}$ relation and corresponding deviation ratio δ for various ϕ and R_0.

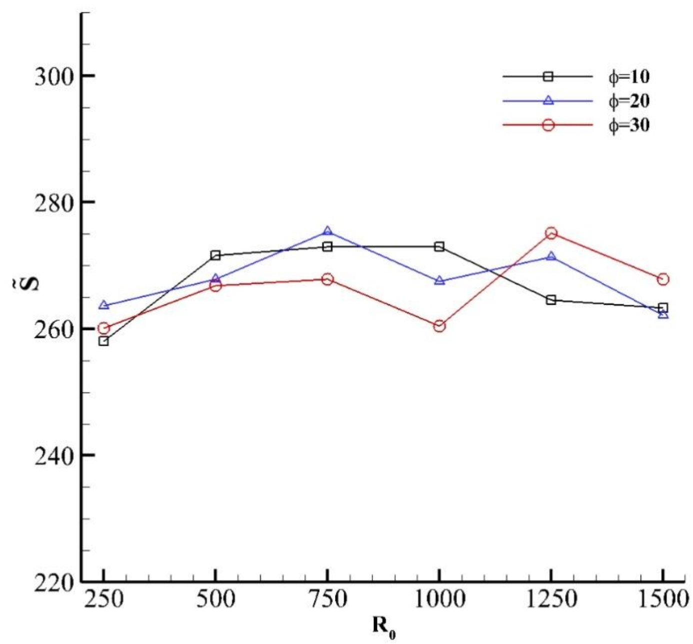

Figure 22: $\tilde{S} - R_0$ relation for various ϕ.